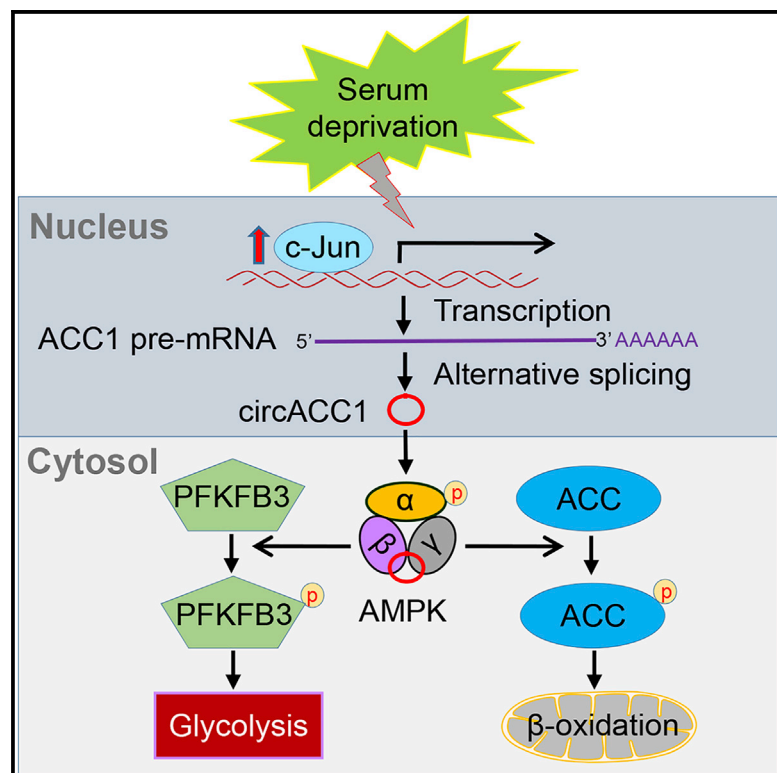


# Cell Metabolism

## CircACC1 Regulates Assembly and Activation of AMPK Complex under Metabolic Stress

### Graphical Abstract



### Authors

Qidong Li, Yichun Wang,  
Shuang Wu, ..., Xu Dong Zhang,  
Wanglai Hu, Mian Wu

### Correspondence

wanglaihu@ahmu.edu.cn (W.H.),  
wumian@ustc.edu.cn (M.W.)

### In Brief

Li et al. demonstrate the mechanism and action of circACC1, a circular RNA derived from preACC1 mRNA, in directly promoting AMPK holoenzyme stability and activation. CircACC1 contributes to metabolic adaptation during serum deprivation by increasing glycolysis and beta-oxidation. Additionally, increased circACC1 may act as a tumor promoter in colorectal cancer.

### Highlights

- CircACC1, a circular RNA, acts as a component of the AMPK holoenzyme
- CircACC1 assembles and stabilizes the AMPK complex and maintains basal activity
- CircACC1 functions in metabolic adaptation responses to serum deprivation
- Elevated circACC1 expression facilitates tumor development *in vitro* and *in vivo*



# CircACC1 Regulates Assembly and Activation of AMPK Complex under Metabolic Stress

Qidong Li,<sup>1</sup> Yichun Wang,<sup>1</sup> Shuang Wu,<sup>6</sup> Zhong Zhou,<sup>1</sup> Xiaojuan Ding,<sup>6</sup> Ronghua Shi,<sup>1</sup> Rick F. Thorne,<sup>2,3,4</sup> Xu Dong Zhang,<sup>2,3,5</sup> Wanglai Hu,<sup>2,3,6,\*</sup> and Mian Wu<sup>1,2,3,7,\*</sup>

<sup>1</sup>The Chinese Academy of Sciences (CAS), Key Laboratory of Innate Immunity & Chronic Disease, CAS Center for Excellence in Cell & Molecular Biology, School of Life Sciences, University of Science & Technology of China, Hefei 230026, China

<sup>2</sup>Translational Research Institute, Henan Provincial People's Hospital, Academy of Medical Science, Zhengzhou University, Zhengzhou 450003, China

<sup>3</sup>Key Laboratory of Stem Cell Differentiation & Modification, School of Clinical Medicine, Henan University, Zhengzhou 450003, China

<sup>4</sup>School of Environmental & Life Sciences, University of Newcastle, Newcastle, NSW 2258, Australia

<sup>5</sup>School of Biomedical Sciences & Pharmacy, University of Newcastle, Newcastle, NSW 2308, Australia

<sup>6</sup>Department of Immunology, Anhui Medical University, Hefei 230027, China

<sup>7</sup>Lead Contact

\*Correspondence: wanglaihu@ahmu.edu.cn (W.H.), wumian@ustc.edu.cn (M.W.)

<https://doi.org/10.1016/j.cmet.2019.05.009>

## SUMMARY

We report that circACC1, a circular RNA derived from human ACC1, plays a critical role in cellular responses to metabolic stress. CircACC1 is preferentially produced over ACC1 in response to serum deprivation by the transcription factor c-Jun. It functions to stabilize and promote the enzymatic activity of the AMPK holoenzyme by forming a ternary complex with the regulatory  $\beta$  and  $\gamma$  subunits. The cellular levels of circACC1 modulate both fatty acid  $\beta$ -oxidation and glycolysis, resulting in profound changes in cellular lipid storage. In a tumor xenograft model, silencing or enforced expression of circACC1 resulted in growth inhibition and enhancement, respectively. Moreover, increased AMPK activation in colorectal cancer tissues was frequently associated with elevated circACC1 expression. We conclude that circACC1 serves as an economic means to elicit AMPK activation and moreover propose that cancer cells exploit circACC1 during metabolic reprogramming.

## INTRODUCTION

During tumor development, energy limitations arising from a nutrient poor microenvironment can exert a selective pressure

on cancer cells (Folkman, 2003; Jones and Thompson, 2009). Indeed, there is increasing evidence that cancer cells are driven to undergo metabolic reprogramming in order to meet the increased demands for energy and metabolites required for rapid cell proliferation and survival (Carracedo et al., 2013; Currie et al., 2013). The first identified and most famous metabolic alteration is the Warburg effect, involving a shift in energy production from oxidative phosphorylation toward accelerated aerobic glycolysis (Bensinger and Christofk, 2012). However, it is now appreciated that cancer cell reprogramming impinges on all metabolic pathways, either directly or as a result of interconnectivity of pathways.

One of the metabolic enzymes that play a crucial role in maintaining energy homeostasis is the AMP-activated protein kinase (AMPK) (Hardie et al., 2012b). AMPK acts as a critical sensor of cellular energy status and plays a multifaceted role in controlling fatty acid oxidation (FAO), glycolysis, and lipolysis (Hardie, 2011; Hardie et al., 2012a; Xie et al., 2006). AMPK has been widely studied in type 2 diabetes and the metabolic syndrome, but given its pivotal role in metabolism, it has also been highlighted as a possible target for cancer treatment (Hardie, 2013). AMPK is a tri-complex consisting of an  $\alpha$  catalytic subunit and  $\beta$  and  $\gamma$  regulatory subunits (Hardie et al., 2012b; Kahn et al., 2005). In response to nutritional or energy stress, AMP binding causes AMPK activation by three complementary mechanisms: (1) allosteric activation; (2) promotion of Thr172 phosphorylation by LKB1 (Hawley et al., 2003; Shaw et al., 2004; Woods et al., 2003), CaMKK2 (Hawley et al., 2005; Hurley et al., 2005; Woods et al., 2005), or TAK1 (Herrero-Martín et al.,

### Context and Significance

Metabolic processes within cells are governed by the extracellular environment. To maintain the balance between energy storage and catabolism, cells utilize an energy-sensing complex called AMPK to respond to fluctuations in nutrients. Here, researchers show that depriving cells of serum switches the production of a linear RNA to a specialized circular form. The circular RNA acts as a constituent part of the AMPK complex and facilitates its activation. This mechanism permits cells to adapt to energy stress and is especially important in cancer, where tumor cells must overcome nutritional deficiencies within the tumor microenvironment. The majority of colon cancers display increased circular RNA levels, suggesting that tumors exploit this mechanism as part of their strategy for growth and survival.



2009; Xie et al., 2006); and (3) inhibition of Thr172 dephosphorylation by protein phosphatases (Davies et al., 1995). Once activated, AMPK minimizes further ATP consumption by suppressing anabolic pathways and activating ATP-generating catabolic pathways (Hardie and Ashford, 2014). Moreover, two other well-characterized AMPK substrates are acetyl-CoA carboxylase-1/2 (ACC1/2) and 6-phosphofructo-2-kinase (PFK2). AMPK-catalyzed phosphorylation results in inactivation of ACC and increased FAO, while phosphorylation activates PFK2 and promotes glycolysis (Carracedo et al., 2013; Marsin et al., 2000).

While different physiological conditions along with post-transcriptional regulatory mechanisms have been identified that influence the expression and activity of AMPK (Jeon, 2016; Zungu et al., 2011), current knowledge of regulatory mechanisms involving non-coding (nc) RNAs is limited. For example, microRNA-451 regulates LKB1-AMPK signaling in glioma cells by directly targeting the LKB1 binding partner CAB39 (Godlewski et al., 2010). Additionally, the long non coding (lnc) RNA NBR2 is upregulated by AMPK in response to energy stress, which in turn interacts with AMPK $\alpha$  to promote AMPK activity (Liu et al., 2016). Moreover, induction of LINC00473 after LKB1 inactivation in lung cancer cells promoted their growth and survival through CREB-mediated transcription (Chen et al., 2016b). None of these examples, however, involve the emerging class of regulatory ncRNAs known as circular (circ)RNAs.

CircRNAs are generated from back-splicing of pre-mRNAs to form covalently closed transcripts. They were originally considered erroneous products of splicing, but it has become clear that circRNAs are discrete functional entities (Memczak et al., 2013; Yu et al., 2017; Zhang et al., 2013). Although circRNAs can arise from introns, the majority of circRNAs consist of varying numbers of constitutive exons rather than alternatively spliced exons. Consequently, circRNA production competes against canonical pre-mRNA splicing and therefore reduces host gene mRNA production (Ashwal-Fluss et al., 2014). Notably, circRNA expression appears to be highly tissue specific (Chuang et al., 2016; Enuka et al., 2016; Rybak-Wolf et al., 2015). Nevertheless, the complexities of circRNA biogenesis as well as the extent of their regulatory functions are yet to be revealed.

Here, we sought to discover roles played by circRNAs in regulating lipid metabolism. Our screening strategy identified a circRNA derived from ACC1 pre-mRNA that we call circACC1. Upon serum deprivation, circACC1 is upregulated by c-Jun and augments the assembly and activity of the AMPK holoenzyme, thereby accelerating  $\beta$ -oxidation and glycolysis. Notably, circACC1 contributes to both basal and 5-aminoimidazole-4-carboxamide ribonucleoside (AICAR) stimulated activities of AMPK. Our study provides insights into how a circular RNA contributes to lipid metabolism through regulating AMPK activity and leads us to propose that circACC1 functions as an economic regulator under metabolic stress to promote  $\beta$ -oxidation and glycolysis. Thus, this mechanism serves to maintain cell integrity by avoiding high-energy-consuming processes such as transcription and translation. Finally, we show that circACC1 promotes the growth of tumor xenografts, and its levels correlate with increased c-Jun and AMPK activation in colorectal cancers.

## RESULTS

### Identification of CircACC1, a Circular RNA Implicated in Lipid Metabolism

We sought to uncover the circRNAs contributing to lipid metabolism by selecting functionally relevant host genes that possess potential for generating circRNAs. We established a matrix of 91 genes known to function in lipid (fatty acid) metabolism (Figure S1A). Using the data of Memczak et al. (2013), which detailed 1,444 validated human circRNAs, we cross-referenced their corresponding parental genes against the 91 genes, deriving a prioritized list of six host genes associated with lipid metabolism, namely *BDH1*, *ACOX1*, *PRKAA1*, *ACC1*, *FABP6*, and *CPT1A* (Figures S1B and S1C). As *CPT1A* can generate two distinctive circRNAs (circCPT1A-1 and CPT1A-2), this provided a total of seven candidates.

We examined whether these circRNAs were present in HCT116 cells, a colon cancer line used as a model for lipid metabolism (Sundqvist et al., 2005). Indeed, pre-digestion of total RNA with RNase R, an exonuclease that selectively degrades linear RNA (Suzuki et al., 2006), before RT-PCR amplification demonstrated that all seven circRNAs were expressed (Figure S1D). Then, as a broad functional screen, we employed small interfering RNA (siRNA) to determine if inhibiting each circRNA led to changes in total cellular lipids. Knockdown of each target showed that depletion of the circRNA generated from *ACC1*, but not others, led to significant lipid accumulation (Figure S1E). We refer to this as circACC1 hereafter.

CircACC1 (hsa\_circ\_001391) is generated from the *ACC1* gene located on human chromosome (chr) 17 with no homology to mouse sequences. The annotation for circACC1 depicts exons 2, 3, and 4 of *ACC1* (total 383 bp) (Glažar et al., 2014). We sought to verify that the form of circACC1 expressed by HCT116 cells matches this report. First, sequencing confirmed that the head-to-tail splice junction was identical to the reported sequence (Figure 1A). Next, the head-to-tail splicing of endogenous circACC1 was assayed by RT-PCR with convergent and divergent primers, along with CDR1as as a control (Hansen et al., 2011). Consistent with the circular form, the divergent primers for circACC1 and CDR1as but not  $\beta$ -actin amplified a PCR product (Figure 1B). To further rule out possibilities that the observed head-to-tail splicing was produced by trans-splicing, genomic rearrangements or even PCR artifacts, we performed northern blotting. This confirmed that circACC1 resolved at  $\sim$ 400 nt consistent with the hsa\_circ\_001391 annotation. Moreover, circACC1 but not  $\beta$ -actin transcripts were resistant to RNase R (Figure 1C). Similarly, qPCR analysis of total RNA after RNase R treatment indicated that circACC1 and CDR1as were resistant, while  $\beta$ -actin and *ACC1* mRNA transcripts were degraded (Figure 1D). Treatment with actinomycin D showed that circACC1 transcripts were stable in comparison to *ACC1* mRNA (Figure 1E). Finally, we excluded the possibility that circACC1 was translated as occurs with some circRNAs through internal ribosome entry sites (IRES) (Yang et al., 2017). An IRES (64–175 bp) was predicted in circACC1, albeit with a low probability score (Chen et al., 2016a), and cloning this region into a split GFP reporter showed that it was unable to mediate translation (Figure 1F). Together, these data established that circACC1 is a *bona fide* circRNA.

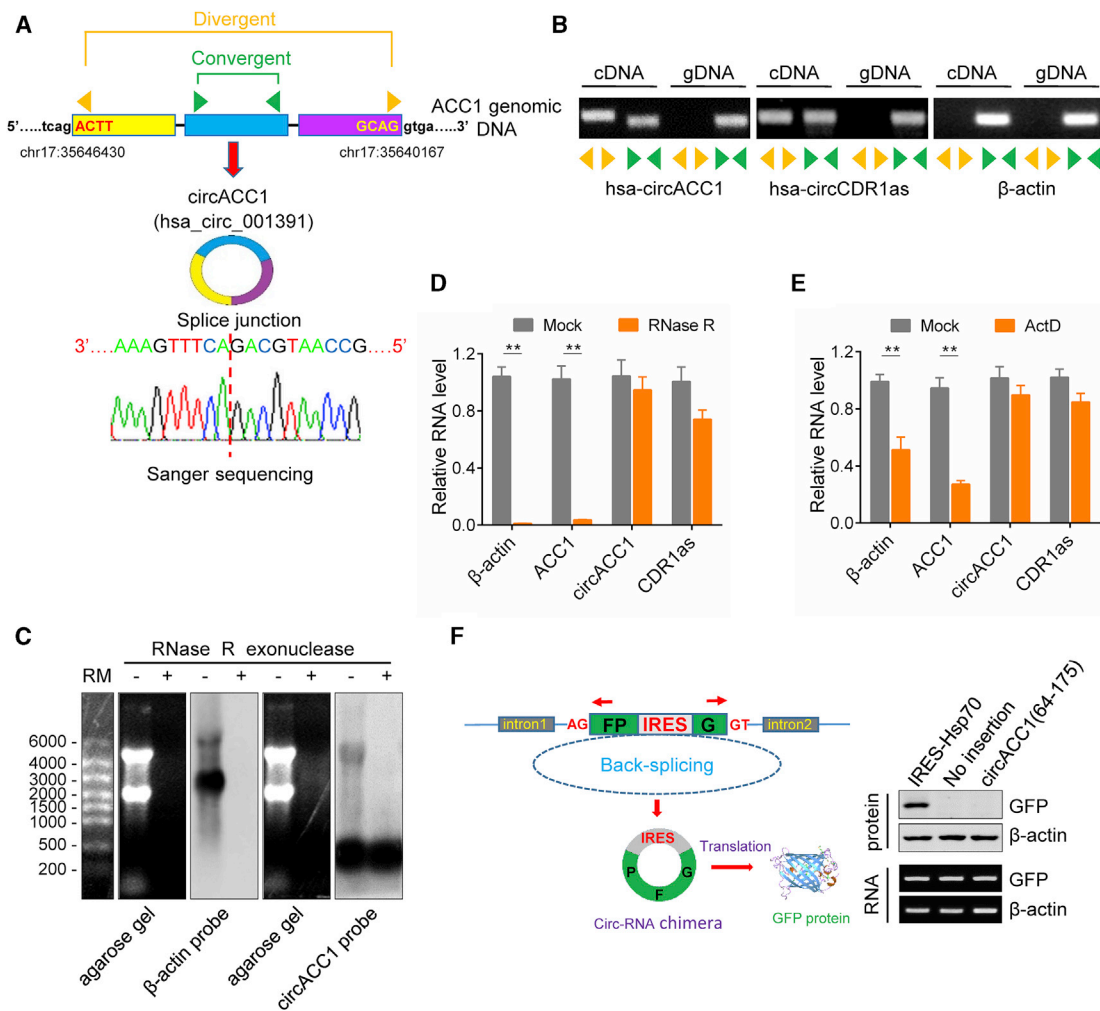


**Figure 1. Identification of CircACC1, a Circular RNA Implicated in Lipid Metabolism**

(A) Sequencing analysis of head-to-tail splicing junction in circACC1.

(B) CircACC1, along with CDR1as and  $\beta$ -actin, was amplified from cDNA or gDNA from HCT116 cells with divergent and convergent primers, respectively.

(C) Northern blotting analysis of circACC1 and  $\beta$ -actin RNA levels in HCT116 cells with and without RNase R treatment.

(D) qPCR assays to determine  $\beta$ -actin, ACC1, circACC1, and CDR1as levels in samples from (C).

(E) Stability of  $\beta$ -actin, ACC1, circACC1, and CDR1as RNA in HCT116 cells with or without 2  $\mu$ g/mL Act D treatment for 24 h compared by qPCR.

(F) Illustration (left) and application of the circRNA translation reporter system in 293T cells (right) using IRES-Hsp70 and circACC1 plasmids.

(A)–(C) represent three independent experiments. (D) and (E) are mean  $\pm$  SD; n = 3 independent experiments, two-tailed Student's t test, \*\*p < 0.01.

### CircACC1 Promotes Glycolysis and FAO

To study the role of circACC1 in greater detail, we expanded our experiments to include overexpression studies along with LO2 cells, a line derived from normal human hepatocytes. Consistent with HCT116 cells, lipid levels were increased in LO2 cells following circACC1 depletion (Figure 2A). In contrast, enforced expression of circACC1 resulted in decreased lipid accumulation in both cell lines (Figure S2A). We next ensured that these were on-target effects resulting from circACC1 silencing. While exons in mRNAs are generally shared with circRNAs (Ashwal-Fluss et al., 2014), head-to-tail splicing in circRNAs gives rise to sequences that are absent in host gene mRNAs. Indeed, knock-down experiments with independent small hairpin RNAs (shRNAs) designed against back-splicing between exons 2 and 4 of circACC1 (Figure 1A) confirmed these selectively targeted

circACC1 but not ACC1 mRNA (Figure S2B). Similar to observations with shRNA, ectopically expressed circACC1 did not affect ACC1 mRNA levels (Figure S2D). Moreover, we verified that ectopically expressed circACC1 was identical to endogenous circACC1 using splice junction overlapping divergent primers (SJOD; Figure S2C). Taken together, these data demonstrate the fidelity of the knockdown and overexpression systems used to manipulate circACC1.

Further lipidomic analyses conducted in parallel with the above experiments revealed that the levels of constituent metabolites present in lipid droplets together with free fatty acids were significantly increased after silencing circACC1 (Figures 2B and 2C, respectively). Considering the parental gene for circACC1 encodes acetyl-CoA carboxylase, a regulator of fatty acid metabolism (Wakil and Abu-Elheiga, 2009), we asked whether

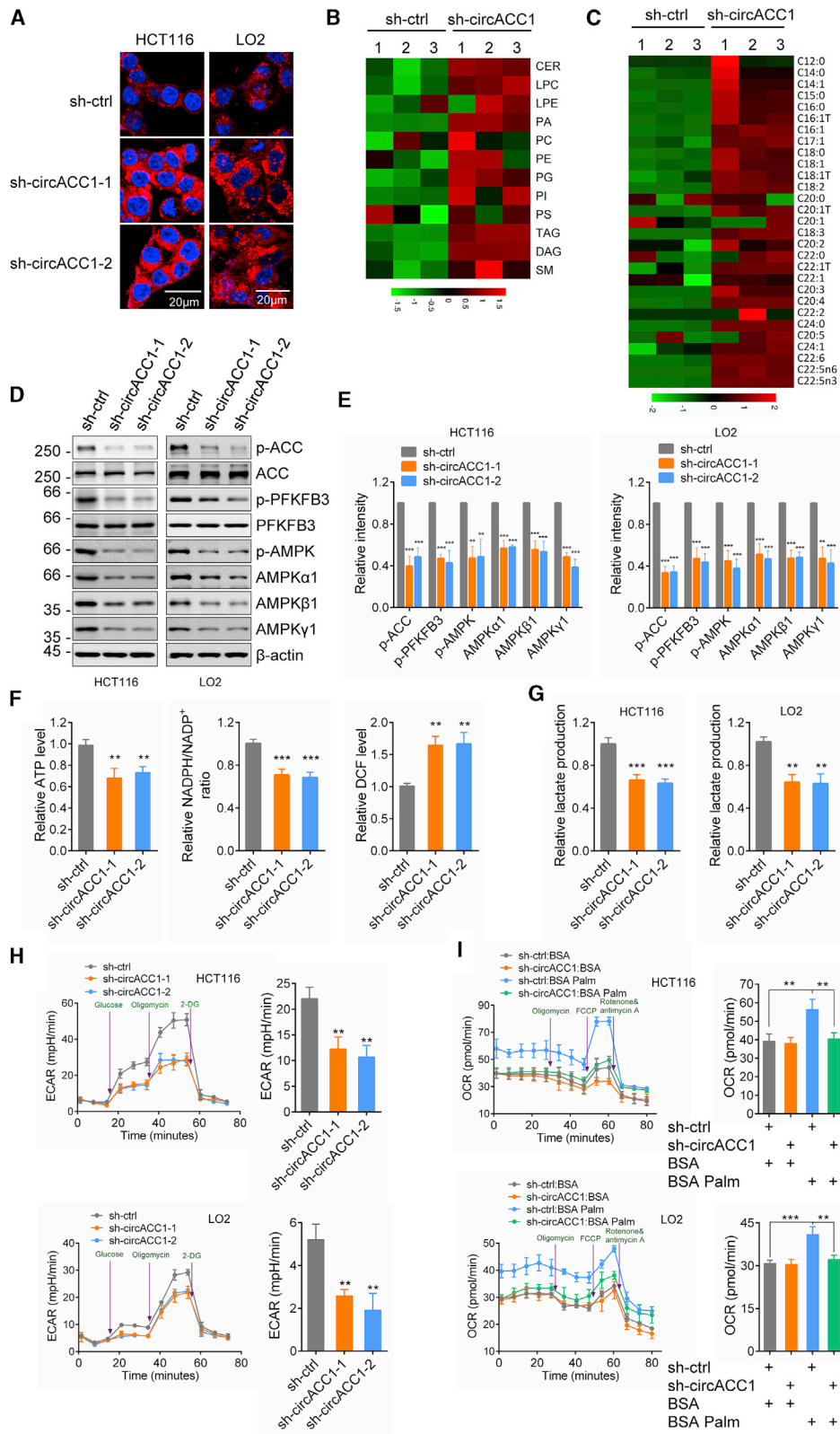


**Figure 2. CircACC1 Promotes Glycolysis and Fatty Acid Oxidation**

(A) Nile red (red) and DAPI (blue) staining of HCT116 and LO2 cells bearing sh-ctrl or sh-circACC1. Representative of three independent experiments. (B and C) Unbiased LC-MS lipid profiles (B) and GC-MS based (C) free fatty acid analysis of HCT116 cells bearing control or circACC1 shRNAs.

(legend continued on next page)

circACC1 affects ACC1 expression or activity. Similar to ACC1 mRNA (Figures S2B and S2D), circACC1 knockdown or overexpression had no effect on ACC1 protein levels (Figures 2D and S2F). Rather, the levels of Thr-172-phosphorylated AMPK and Ser79-phosphorylated ACC1 were markedly decreased when circACC1 was silenced. Moreover, there were also decreased levels of the catalytic  $\alpha$  and non-catalytic  $\beta$  and  $\gamma$  subunits of AMPK (Figures 2D and 2E). This was not mediated through transcriptional changes, as depleting circACC1 did not influence their mRNA levels (Figure S2E). Consistently, overexpression of circACC1 promoted increased phosphorylation of AMPK and ACC1 with accompanying increased levels of AMPK  $\alpha$ ,  $\beta$ , and  $\gamma$  (Figures S2F and S2G). As it is known that AMPK phosphorylates ACC1 on Ser79 to inhibit its enzymatic activity (Fullerton et al., 2013), these data propose that circACC1 serves to influence ACC1 activity through effects on AMPK expression and activity. Nevertheless, these data do not exclude the possibility that circACC1 may directly antagonize ACC1. We therefore investigated the function of circACC1 in the AMPK pathway.

AMPK functions to maintain energy homeostasis, remedying low intracellular ATP levels by promoting glycolysis and increasing FAO (Hardie, 2011). In response to energy stress, AMPK phosphorylates and activates PFK-2, which serves to stimulate glycolysis (Marsin et al., 2000, 2002), whereas AMPK inhibits fatty acid synthesis (FAS) and stimulates FAO via the phosphorylation of ACC1 and ACC-2, respectively (Hardie and Pan, 2002). AMPK may also indirectly contribute to NADPH maintenance since there is decreased utilization of NADPH in FAS and increased NADPH production via FAO when AMPK is activated (Jeon et al., 2012). Knockdown of circACC1 not only decreased phosphorylation of ACC1 but also significantly decreased Ser461 phosphorylation of PFKFB3, one of two PFK2 isoforms regulated by AMPK (Marsin et al., 2000; Marsin et al., 2002) and a proxy measure of PFK2 activation (Figures 2D and 2E). Conversely, overexpression of circACC1 increased PFKFB3 phosphorylation (Figures S2F and S2G). As further verification, we generated a shRNA-resistant construct (circACC1R) and confirmed that its ectopic expression rescued inhibition of AMPK activity observed after knockdown of endogenous circACC1 (Figure S2H). Consistent with the projected effects of altered AMPK signaling, silencing of circACC1 decreased the cellular levels of ATP, NADPH, and extracellular lactate while increasing reactive oxygen species (ROS) levels, whereas forced expression of circACC1 produced entirely opposite effects (Figures 2F, 2G, S2I, and S2J, respectively). Collectively, these data support the hypothesis that circACC1 functions to enhance AMPK activity that, in turn, promotes glycolysis and FAO.

To further test this idea, we performed extracellular acidification rate (ECAR) and oxygen consumption rate (OCR) assays,

used as proxy measures of glycolytic flux and mitochondrial respiration, respectively. As anticipated, knockdown of circACC1 significantly reduced ECAR in HCT116 and LO2 cells (Figure 2H). Moreover, the increased OCR observed after supplementing the cells with exogenous free fatty acids (FFA; palmitate) was ablated when circACC1 was silenced (Figure 2I). Conversely, overexpression of circACC1 significantly increased ECAR along with increased OCR and FFA utilization (Figures S2K and S2L, respectively). Collectively, these data support the role of circACC1 in regulating AMPK activity and imparting effects on glycolysis and FAO and reconcile with the changes in lipid accumulation after manipulating circACC1 (Figures 2A and S2A).

### Circ-ACC1 Directly Binds to AMPK $\beta$ and $\gamma$ Subunits

The aforementioned results prompted us to study how circACC1 regulates AMPK function. We first determined that individual AMPK subunits along with circACC1 were predominately cytoplasmic (Figures 3A–3C). RNA pull-down assays were then used to determine if there were direct interactions between circACC1 and AMPK subunits. Indeed, each subunit of AMPK was selectively captured with antisense but not sense probes directed against circACC1 (Figure 3D). However, as AMPK exists as an  $\alpha$ - $\beta$ - $\gamma$  complex *in vivo* (Woods et al., 1996), this assay did not distinguish if circACC1 forms a complex with the AMPK holoenzyme or alternatively interacts with individual subunits. Thus, we examined how circACC1 interacts with AMPK subunits by transfection of individual FLAG-tagged  $\alpha$ 1,  $\beta$ 1, and  $\gamma$ 1 subunits into HCT116 cells. RNA immunoprecipitation (RIP) analysis revealed that circACC1 interacted strongly with AMPK  $\beta$ 1 and  $\gamma$ 1 subunits but showed minimal binding to  $\alpha$ 1 (Figure 3E). In support, RIP assays performed against endogenous  $\beta$ 1 and  $\gamma$ 1 confirmed their interaction with circACC1 (Figure 3F).

On this basis, we investigated if interactions between circACC1 and AMPK  $\beta$ 1 and  $\gamma$ 1 were involved in holoenzyme assembly. We conducted two-step immunoprecipitation after transfection of FLAG-AMPK $\gamma$ 1 and HA-AMPK $\beta$ 1. In the first phase, anti-FLAG antibodies precipitated FLAG-AMPK $\gamma$ 1 along with  $\alpha$ 1,  $\beta$ 1, and circACC1 from total protein extracts, whereas the secondary IP against HA-AMPK $\beta$ 1 captured  $\alpha$ 1,  $\gamma$ 1, and circACC1 (Figure 3G). These data are indicative of a tetramer formed between the AMPK holoenzyme and circACC1. Reconstructing these interactions *in vitro* demonstrated that immunopurified AMPK $\beta$ 1 and  $\gamma$ 1, but not  $\alpha$ 1, was able to co-precipitate with cyclized biotin-labeled circACC1 (Figure 3H). Importantly, circACC1 was also shown to interact with bacterially produced AMPK $\beta$ 1 and  $\gamma$ 1 but not  $\alpha$ 1 (Figure S3A), confirming the findings with AMPK subunits purified from mammalian cells (Figure 3H). Moreover, the interaction of AMPK $\beta$ 1 or  $\gamma$ 1 with circACC1 was

(D and E) Western blotting of HCT116 and LO2 cells expressing sh-ctrl or sh-circACC1 using the indicated antibodies (D) and quantification using ImageJ software (E).

(F) Total ATP levels, NADPH/NADP<sup>+</sup> ratio and ROS were measured in HCT116 cells from (D).

(G) Extracellular lactate production in HCT116 and LO2 cells from (D).

(H) ECAR was measured by Seahorse XF assays in HCT116 (top) and LO2 (bottom) cells from (D).

(I) OCR was measured by Sea horse XF assays in HCT116 (top) and LO2 cells (bottom) bearing sh-ctrl or sh-circACC1 without and with addition of exogenous fatty acids. Basal OCR levels during the first 30 min at right.

(E)–(I) are mean  $\pm$  SD; n = 3 independent experiments. (E–H) one-way ANOVA with Tukey's multiple comparison post-test; (I) two-way ANOVA with Bonferroni's multiple comparison post-test, \*\*p < 0.01, \*\*\*p < 0.001.

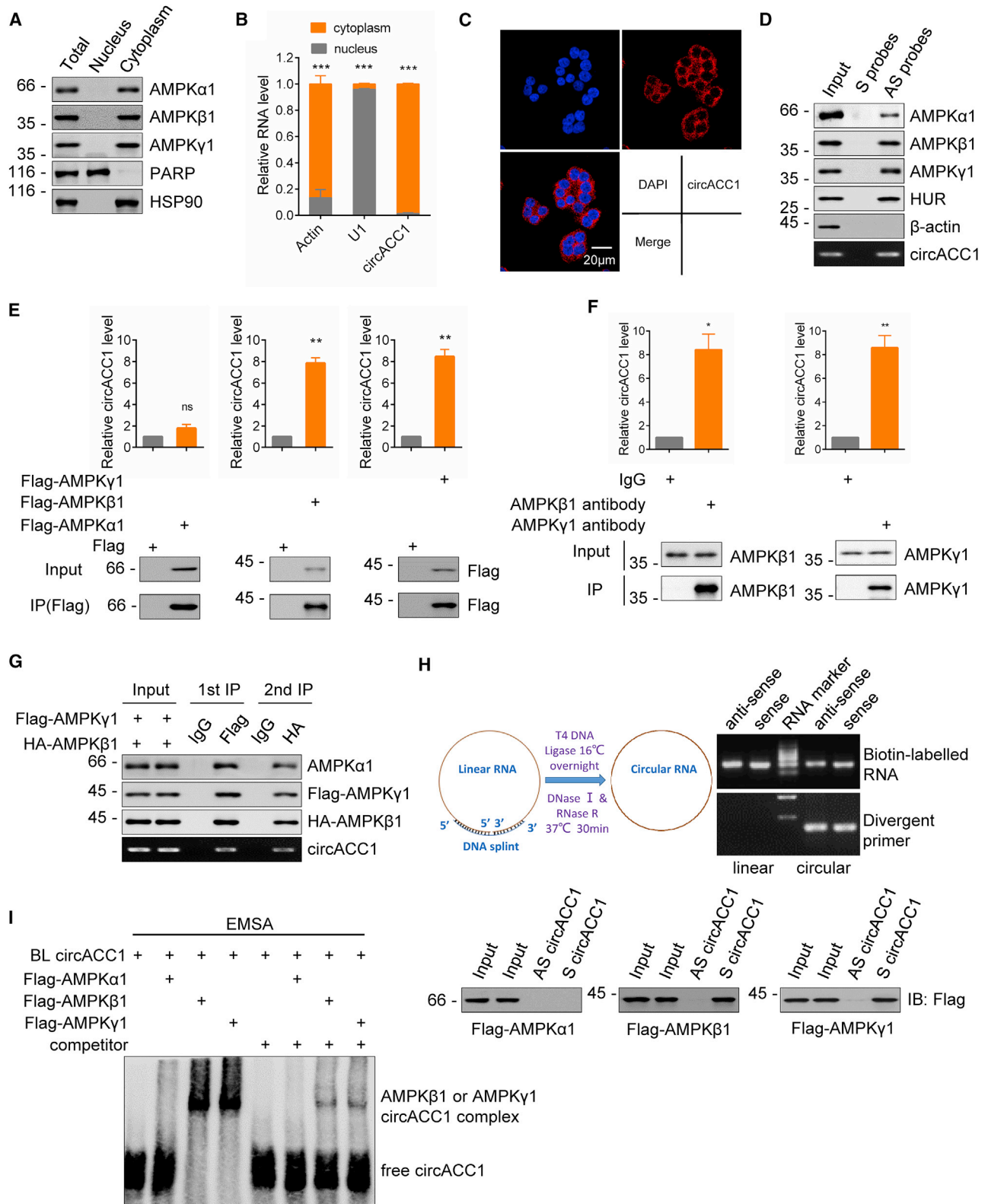


**Figure 3. CircACC1 Directly Binds to AMPK β and γ Subunits**

(A and B) Subcellular fractionation of HCT116 cells and measurement of AMPK subunits by western blotting (A) and circACC1 by qPCR (B).

(C) FISH detection of circACC1 in HCT116 cells.

(D) Biotin-labeled sense (S) or antisense (AS) circACC1 probes were used for RNA-protein pull-down against HCT116 cell lysates.

(legend continued on next page)

readily detected by supershift in electrophoretic mobility shift assays (Figure 3I).

To delineate the structural determinants of the interactions between circACC1 and AMPK subunits, we carried out deletion mapping by subdividing the AMPK $\beta$ 1 and  $\gamma$ 1 functional domains (Lin and Hardie, 2018; Oakhill et al., 2012). RNA pull-down assays showed that removal of the  $\gamma$  binding domain (aa227-270) of AMPK $\beta$ 1 abolished its association with circACC1 (Figure S3B), while deletion of the N terminus (aa1-43) of AMPK $\gamma$ 1 diminished its interaction with circACC1 (Figure S3C). Thus, circACC1 interacts with C- and N-terminal domains of AMPK $\beta$ 1 and  $\gamma$ 1, respectively. The secondary structure of circACC1 based on minimum free energy predicts that circACC1 is bipolar (Figure S3D). On this basis, we divided circACC1 into two fragments, P1 (nt 1–184) and P2 (nt 185–383). Repeating the RNA pull-down assays showed that P1 but not P2 supported circACC1 binding to AMPK $\beta$  and  $\gamma$  (Figure S3D). We then further dissected P1 by deleting nt 1–97 (circACC1 $\Delta$ P1a) or nt 98–184 (circACC1 $\Delta$ P1b) (Figure S3D). Instructively, circACC1 $\Delta$ P1b selectively lost AMPK $\beta$ 1-binding activity, whereas circACC1 $\Delta$ P1a could no longer bind to AMPK $\gamma$ 1 (Figure S3D); thus, discrete regions in circACC1 are responsible for binding.

### CircACC1 Facilitates AMPK Holoenzyme Assembly, Stability, and Activity

We returned to consider how circACC1 exerts its effects on AMPK signaling. Prior experiments showed circACC1 knockdown triggered marked reduction in protein levels of each AMPK subunit (Figure 2D). Proteasomal inhibition stabilized the levels of all AMPK subunits following circACC1 silencing, suggesting that circACC1 influences protein stability (Figure 4A). In support, circACC1 knockdown markedly reduced the half-life of individual AMPK subunits in cycloheximide chase assays (Figure S4A). Moreover, circACC1 knockdown increased AMPK subunit poly-ubiquitination (Figure 4B), suggesting that circACC1 acts to prevent AMPK ubiquitination and proteasomal degradation.

An intriguing observation was that manipulating circACC1 affected all AMPK subunits, although circACC1 only binds to AMPK  $\beta$ 1 and  $\gamma$ 1. This proposes that the primary role of circACC1 is to facilitate the assembly and/or maintain stability of the AMPK holoenzyme. The corollary to this is that an equilibrium is maintained because unassociated AMPK subunits are vulnerable to degradation. Indeed, phenocopying the effects of circACC1 silencing (Figure 2D), knockdown of individual AMPK  $\alpha$ 1,  $\beta$ 1, and  $\gamma$ 1 subunits lead to greatly diminished the levels of other subunits (Figure S4B). After stabilizing protein levels with MG132, the relative amount of co-association between endogenous AMPK subunits was reduced in circACC1 knockdown

cells, indicating the presence of less holoenzyme (Figure 4C). Furthermore, consistent with prior transfection experiments (Figure 3E), *in vitro* transcribed circACC1 enhanced the binding between AMPK  $\beta$ 1 and  $\gamma$ 1 subunits but not others (Figure 4D).

As a complementary approach, we turned to the mammalian two-hybrid system used to study protein-protein interactions *in vivo*. Bait (BD) and prey (AT) fusion vectors were constructed to test interactions between AMPK subunits. Measuring protein-protein interactions by reporter assays showed that circACC1 silencing reduced only the interaction between AMPK  $\beta$ 1 and  $\gamma$ 1 subunits but not other interactions (Figure 4E). Consistently, circACC1 overexpression selectively enhanced binding between AMPK  $\beta$ 1 and  $\gamma$ 1 subunits (Figure S4C). Together, these results show that circACC1 facilitates AMPK holoenzyme assembly and stability.

Finally, we sought to confirm the relationship between circACC1, activation of the AMPK holoenzyme, and inactivation of ACC1. We evaluated this by reconstituting interactions in a cell-free system employing recombinant ACC1 and AMPK protein subunits along with *in vitro* synthesized circACC1 (Figure 4F). Here, the presence of circACC1 was equivalent to treating the reaction with the AMPK-specific activator A-769662. The levels of pACC1 were selectively increased in the presence of circACC1, phenocopying the effects of A-769662, which activates AMPK through an allosteric mechanism (Göransson et al., 2007). Notably, AMPK could not be activated by circACC1 when an A-769662-insensitive AMPK $\beta$  (S108A) mutant (Sanders et al., 2007) was used (Figure S4D). The application of the conditional binding mutants circACC1 $\Delta$ P1a and circACC1 $\Delta$ P1b also failed to support an increase in pACC1 levels (Figure 4G). Moreover, circACC1 $\Delta$ P1a and circACC1 $\Delta$ P1b neither promoted increases in phosphorylated ACC1 or AMPK nor increased the levels of AMPK subunits (Figure 4H). Collectively, these data propose that circACC1 is required for both stabilization and activation of AMPK.

### CircACC1 Maintains AMPK Basal Activity and Functions in an AMPK-Dependent Manner

The role of AMPK signaling involves sensing and responding to changes in cellular energy and nutrient status. We thus examined how various metabolic stress conditions influenced circACC1 expression. RT-PCR analysis revealed that circACC1 was upregulated upon serum removal but not glucose, glutamine, or serine deprivation (Figure 5A). Furthermore, levels of pre-ACC1 RNA and circACC1, but not mature ACC1 mRNA, were selectively induced by serum deprivation in both HCT116 and LO2 cells (Figures 5B and 5C), indicating that circACC1 is preferentially produced over ACC1 mRNA under metabolic stress conditions. Notably, circACC1 expression levels were restored to

(E) Immunoprecipitation analysis of HCT116 cells after FLAG-AMPK  $\alpha$ -1,  $\beta$ 1, or  $\gamma$ 1 transfection using anti-FLAG antibodies or IgG control.

(F) RIP assays in HCT116 cells using AMPK $\beta$ 1 or AMPK $\gamma$ 1 antibodies.

(G) HCT116 cells co-transfected with FLAG-AMPK $\beta$ 1 and HA-tagged were used to perform sequential immunoprecipitations with anti-FLAG and anti-HA antibodies.

(H) Schematic illustrating cyclization of linear RNA generated *in vitro* (top). RT-PCR analysis of linear and cyclized circACC1 RNAs with SJOD primers (middle). RNA-protein pull-down assays were conducted in 293T cells transfected with FLAG-AMPK $\alpha$ 1,  $\beta$ 1, or  $\gamma$ 1 against cyclized circACC1 (bottom).

(I) Electrophoretic mobility shift analysis of interactions between circACC1 and FLAG-AMPK  $\alpha$ -1,  $\beta$ 1, or  $\gamma$ 1.

Data in (A), (C), (D), and (G–I) representative of three experiments; (B, E, and F) mean  $\pm$  SD from 3 independent experiments, two-tailed paired Student's *t* test, ns, not significant, \**p* < 0.05, \*\**p* < 0.01, \*\*\**p* < 0.001.

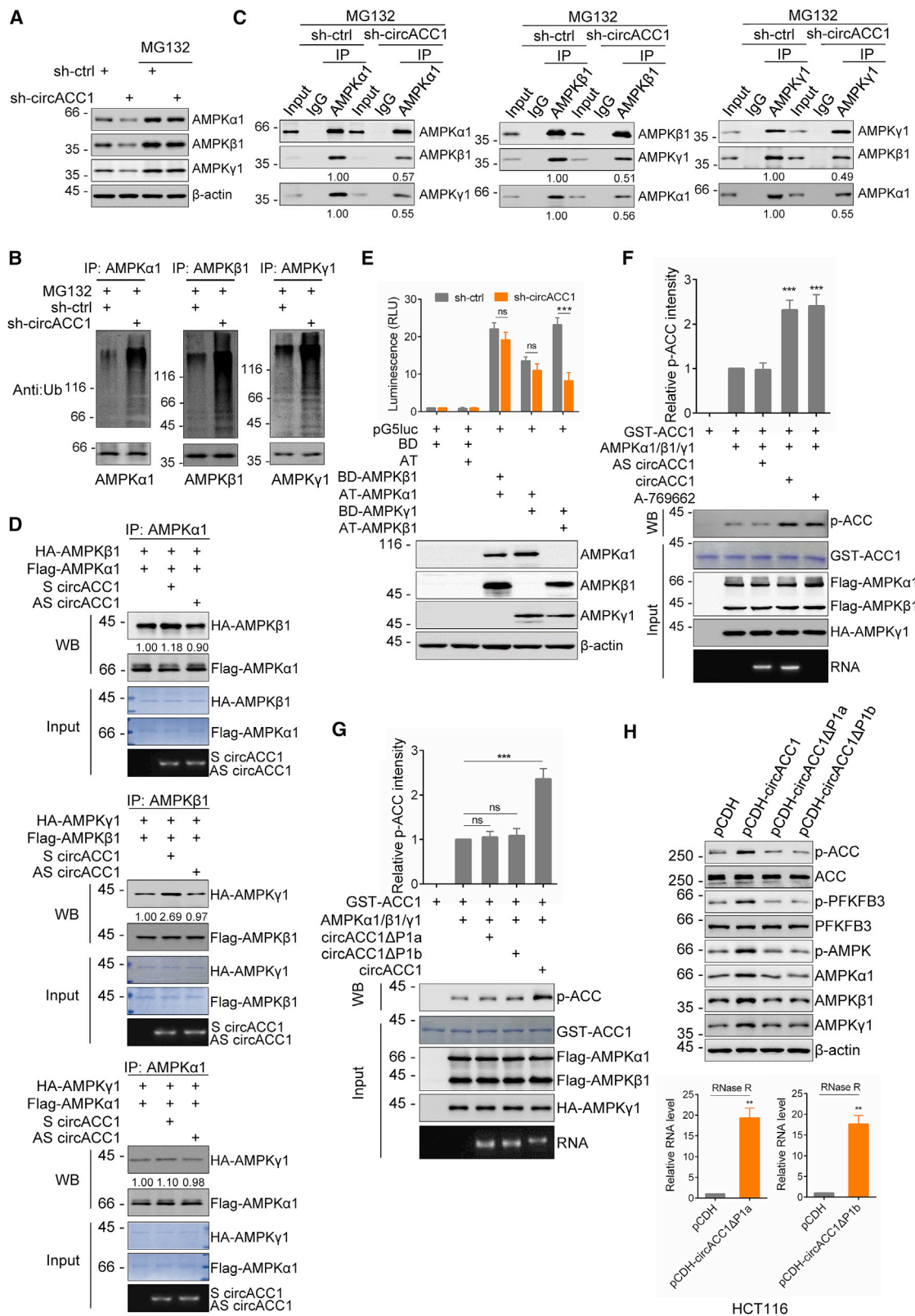


**Figure 4. CircACC1 Facilitates AMPK Holoenzyme Assembly, Stability, and Activity**

(A) HCT116 cells bearing sh-ctrl or sh-circACC1 were treated with or without 10 μM MG132 for 12 h, and the levels of AMPK subunits were compared by western blot.

(legend continued on next page)

baseline after supplementing deprived cells with serum, showing that circACC1 is regulated by serum availability (Figure 5D). Consistently, digital droplet PCR confirmed that serum deprivation caused a ~3- to 4-fold increase in circACC1 levels, corresponding to an estimated 300–400 copies of circACC1 per cell (Figure 5E).

AMPK is known to be activated *in vivo* by several different kinases including LKB1, CaMKK2, and TAK1 by promoting Thr172 phosphorylation (Hawley et al., 2003, 2005; Herrero-Martín et al., 2009; Hurley et al., 2005; Shaw et al., 2004; Woods et al., 2005, 2003). We then asked whether the role of circACC1 in the modulation of AMPK activity was dependent on these kinases. As anticipated, knockdown of LKB1, CaMKK2, and TAK1 by shRNA reduced AMPK and PFKFB3 activation and decreased the phosphorylation of ACC1. Nevertheless, ectopic expression of circACC1 resulted in modest increases in activation of AMPK, irrespective of whether LKB1, CaMKK2, or TAK1 were expressed (Figure 5F). Similarly, circACC1 was shown to activate AMPK in both HeLa and A549 cells, in which *LKB1* alleles were known to be homozygous null (Figure 5G). However, it has been previously reported that no AMPK activity can be detected if both LKB1 and CaMKK2 are deleted (Willows et al., 2017). We repeated these experiments following the double knockdown of LKB1 and CaMKK2 in HCT116 cells or the knockdown of CaMKK2 in HeLa cells (Figures S5A and S5B, respectively). Consistently, activation of AMPK, ACC1, and PFKFB3 was almost undetectable in cells lacking LKB1 and CaMKK2, and moreover, only a weak activation occurred after enforced expression of circACC1. These data demonstrate that although circACC1 is able to enhance the basal activity of AMPK, classical upstream regulatory kinases are still required for its activation. We also assessed circACC1 actions in the presence of AICAR, a commonly used AMPK agonist (Corton et al., 1995). Notably, knockdown of circACC1 was able to significantly blunt AICAR-induced activation of AMPK along with its downstream activation (Figure S5C). Thus, circACC1 actions are similarly relevant for AMPK in an activated state.

We next sought to confirm whether the effects of circACC1 on lipid metabolism and glycolysis were mediated through AMPK. As anticipated, knockdown of AMPK $\alpha$  in HCT116 cells reduced AMPK activation and phosphorylation of ACC1. Nevertheless, ectopic expression of circACC1 failed to rescue the phenotype induced by AMPK $\alpha$  knockdown (Figure S5D). Alternatively, we also applied constitutively active (CA) T172D AMPK $\alpha$ 1 (amino acids [aas] 1–312) to test whether this would rescue the changes observed in circACC1-deficient cells. Indeed, overexpression of CA-AMPK in circACC1 knockdown cells restored AMPK activation and phosphorylation of ACC1 (Figure S5E). Together, these

data establish that the functional effects of circACC1 are dependent on AMPK.

Finally, we established if circACC1-mediated regulation of AMPK was specific for either AMPK  $\alpha$ 1 or  $\alpha$ 2-subtype complexes. We identified that AMPK $\alpha$ 1 but not  $\alpha$ 2 was induced by serum removal, suggesting that circACC1 likely functions through  $\alpha$ 1 (Figure S5F). Indeed, circACC1 was unable to bind to AMPK $\alpha$ 2-containing complexes in RNA pull-down assays (Figure S5G). Thus, the function of circACC1 under serum deprivation is AMPK $\alpha$ 1 subtype specific.

### C-Jun Increases CircACC1 Production in Response to Serum Deprivation

Analysis of the promoter of *ACC1* revealed binding motifs for CEBPA, c-Jun, CREB1, and SREBF1 (Figure S6A), transcription factors with established functional relationships with metabolic regulation (Altarejos and Montminy, 2011; Damiano et al., 2010; Lamph et al., 1988; Lu et al., 2015). To ascertain whether these transcription factors were involved in circACC1 regulation, we performed knockdown studies. Unequivocally, silencing of c-Jun but not others significantly decreased circACC1 expression under serum deprivation (Figure S6B), indicating that c-Jun was responsible for circACC1 upregulation. Indeed, direct binding of endogenous activated (Ser73-phosphorylated) c-Jun to the *ACC1* promoter was confirmed using chromatin immunoprecipitation (ChIP) (Figures 6A and 6B). The c-Jun motif is located upstream (-339 to -333 bp) of the *ACC1* translational start site (Figure 6A). Transfection of c-Jun enhanced the transcriptional activity of a luciferase reporter containing the c-Jun binding site, whereas mutation of this sequence completely abolished the increased activity, confirming that the -339 to -333 region is responsible for c-Jun binding (Figures 6A and 6C). Consistently, the mutated c-Jun reporter failed to increase luciferase activity upon serum deprivation (Figure 6D). Furthermore, treatment of serum-deprived cells with DB07268, a specific JNK inhibitor, reversed the increase in both pre-ACC1 expression and circACC1 production (Figure S6C). Thus, the expression of circACC1 appears to be c-Jun dependent. Indeed examining a cell line panel showed good concordance between the levels of activated c-Jun and circACC1 expression (Figure S6D).

The JNK pathway has been shown to be activated under serum-deprivation conditions (Davis, 2000; Jiang et al., 2017), and we confirmed that serum deprivation induced c-Jun activation in a time-dependent manner, along with increases in phosphorylated JNK and AMPK signaling and decreased ACC1 activity (Figure 6E). Instructively, knockdown of c-Jun in serum-deprived cells phenocopied the effects of circACC1

(B) Polyubiquitination of AMPK subunits was analyzed in HCT116 cells from (A).

(C) Immunoprecipitation analysis of the association between AMPK subunits in MG132-treated HCT116 cells bearing sh-ctrl and sh-circACC1.

(D) *In vitro* binding between recombinant AMPK subunits purified from 293T cells was analyzed in the presence and absence of circACC1.

(E) Mammalian two-hybrid assays measuring interactions between AMPK subunits in the presence and absence of endogenous circACC1.

(F and G) Recombinant AMPK was assembled *in vitro* and AMPK kinase activity measured in the presence and absence of circACC1 (F) or circACC1, circACC1 $\Delta$ P1a, or circACC1 $\Delta$ P1b (G).

(H) HCT116 cells expressing the indicated plasmids were analyzed by western blotting (top) and the levels of the circACC1 conditional binding mutants measured after RNase R treatment (bottom).

(E) Two-way ANOVA with Bonferroni's multiple comparison post-test, (F and G) one-way ANOVA with Tukey's multiple comparison post-test, (H) two-tailed paired Student's *t* test, ns, not significant, \*\**p* < 0.01, \*\*\**p* < 0.001.

(A)–(D) are representative of three independent experiments. Data in (E–H) are mean  $\pm$  SD, *n* = 3 independent experiments.

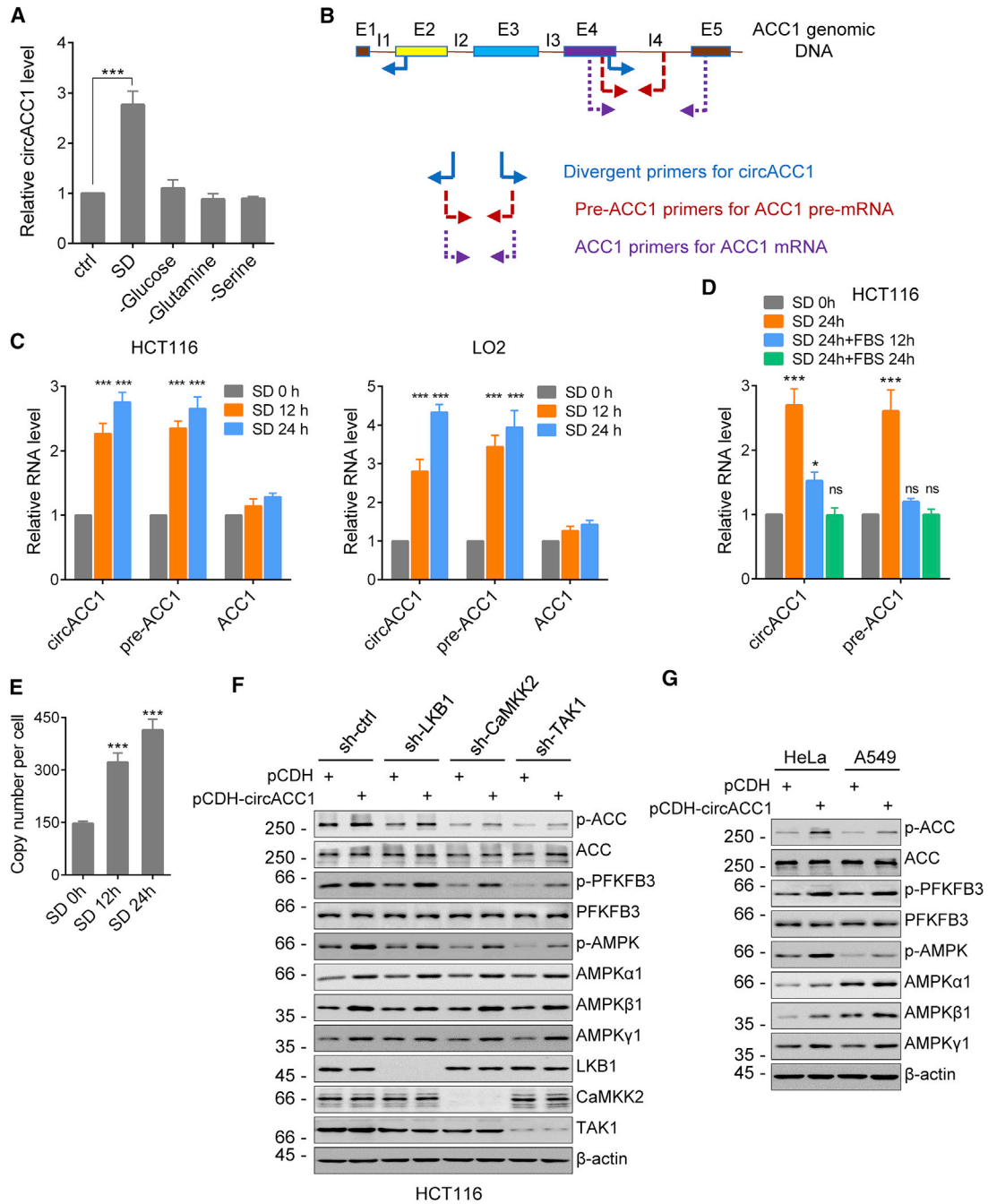


**Figure 5. CircACC1 Maintains AMPK Basal Activity and Functions in an AMPK-Dependent Manner**

(A) CircACC1 abundance determined by qPCR in HCT116 cells after 24 h of the indicated stress conditions (SD, serum deprivation).

(B and C) Strategy to distinguish between circACC1, pre-ACC1, and ACC1 mRNA using qPCR (B) and their analysis in HCT116 and LO2 cells after 0–24 h of serum deprivation (C).

(D) qPCR analysis of circACC1 and pre-ACC1 conducted in HCT116 cells as per (C) after the indicated culture conditions.

(E) Quantitation of circACC1 by digital droplet PCR in HCT116 cells after serum deprivation.

(F) Western blot analysis of HCT116 cells expressing pCDH or pCDH-circACC1 in combination with sh-central or knockdown of LKB1, CaMKK2, or TAK1 as indicated.

(G) *LKB1*-deficient cell HeLa and A549 cells overexpressing pCDH or pCDH-circACC1 were analyzed as per (F).

Data in (A) and (C)–(E) are mean ± SD; n = 3 independent experiments.

(A) and (C)–(E) one-way ANOVA with Tukey's multiple comparison post-test, ns, not significant, \*p < 0.05, \*\*\*p < 0.001.

(F and G) are representative of three independent experiments.

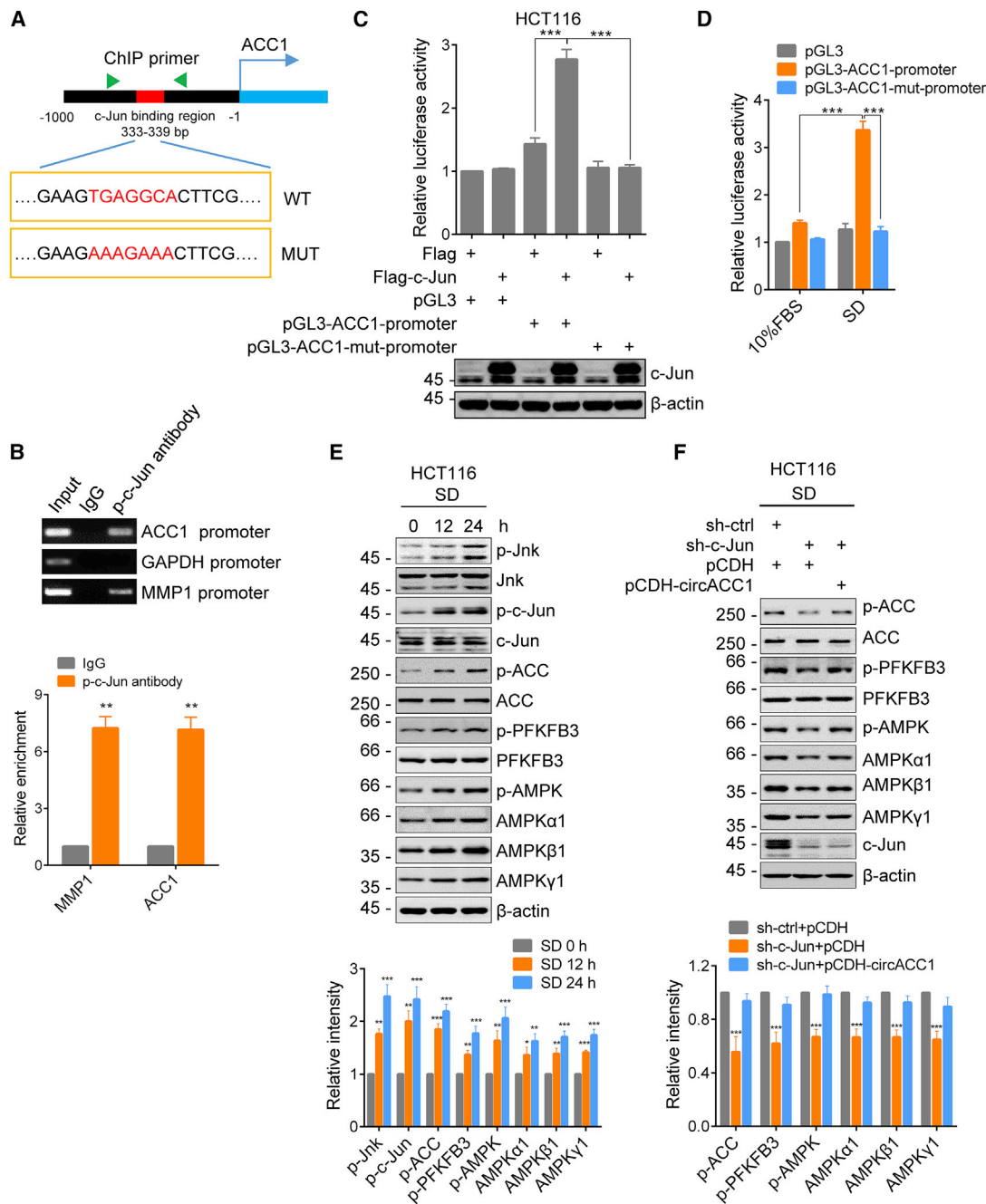


**Figure 6. C-Jun Increases CircACC1 Production in Response to Serum Deprivation**

(A) Schematic of the putative c-Jun binding site in the *ACC1* promoter and the strategy for ChIP analysis. The consensus and mutant sequences for c-Jun binding are boxed.

(B) ChIP assays conducted in HCT116 cells using anti-p-c-Jun (Ser73) antibodies or control IgG.

(C) Luciferase reporter assays in HCT116 cells after co-transfection of the indicated plasmids for 24 h.

(D) Luciferase reporter assays were conducted as per (C) after 24 h serum deprivation.

(E) Western blot analysis of HCT116 cells cultured under serum-free conditions for 0, 12, or 24 h comparing the indicated proteins (top) and their relative levels determined using ImageJ (bottom).

(F) HCT116 cells bearing sh-ctrl or sh-c-Jun were transfected with pCDH or pCDH-circACC1 plasmids as indicated and then cultured under serum-free conditions for 24 h before conducting analyses as per (E).

(B) Two-tailed paired Student's t test.

(C and D) Two-way ANOVA with Bonferroni's multiple comparison post-test.

(E and F) One-way ANOVA with Tukey's multiple comparison post-test, \* $p < 0.05$ , \*\* $p < 0.01$ , \*\*\* $p < 0.001$ .

Data shown in (B)–(F) are mean  $\pm$  SD;  $n = 3$  independent experiments.

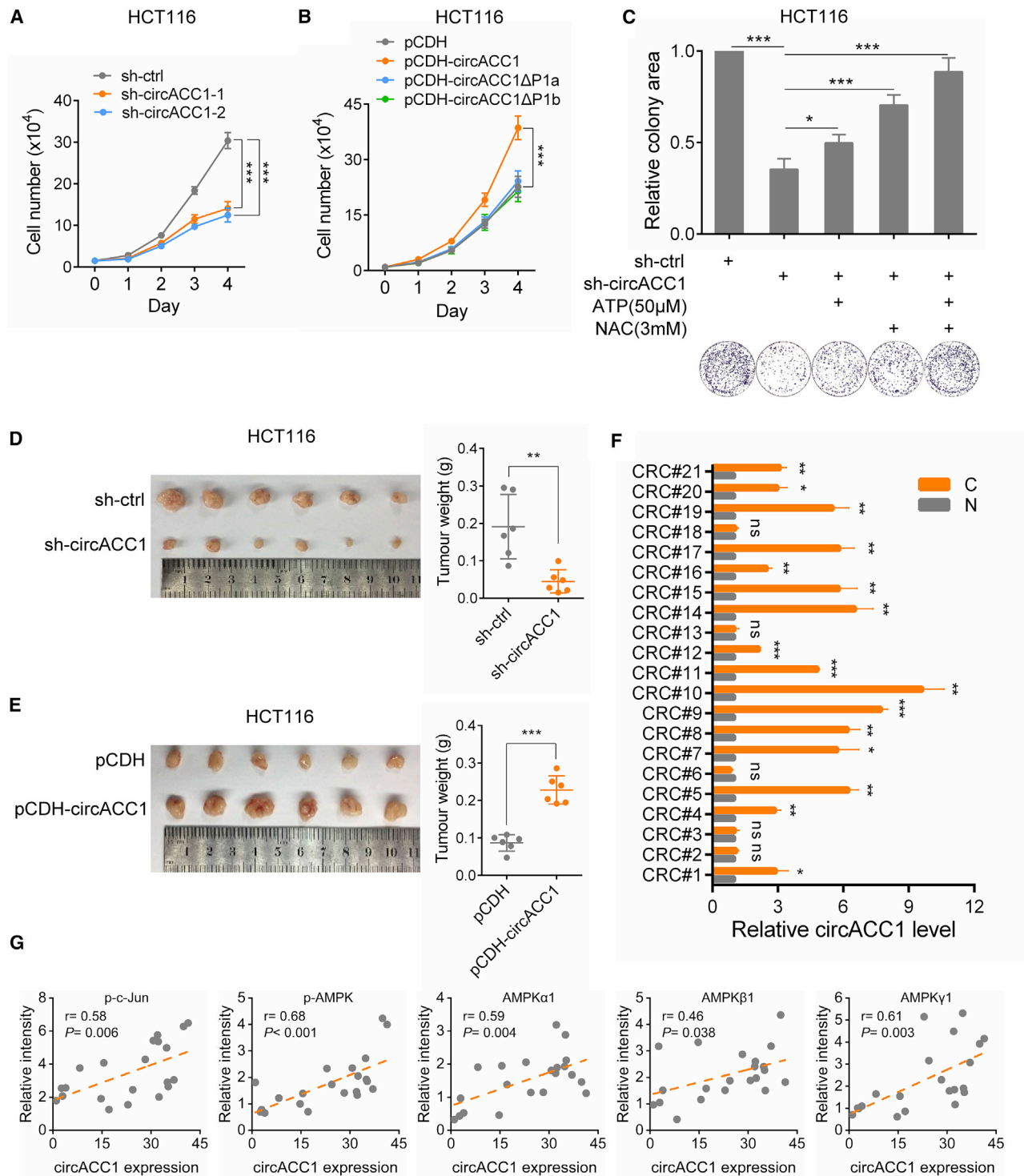


**Figure 7. Biological Implications of CircACC1 in Tumorigenesis**

(A and B) Comparison of cell proliferation rates in HCT116 cells after knockdown of circACC1 (A) or ectopic expression of circACC1, circACC1 $\Delta$ P1a, or circACC1 $\Delta$ P1b (B).

(C) HCT116 cells expressing sh-ctrl or sh-circACC1 in combination with the indicated treatments were subjected to clonogenic assays.

(D and E) Comparison of the growth of HCT116 xenografts expressing sh-ctrl versus sh-circACC1 (D) or pCDH versus pCDH-circACC1 (E).

(F) qPCR analysis of circACC1 among 21 pairs of matched colorectal cancer and adjacent normal tissue.

(legend continued on next page)

depletion with reduced AMPK signaling and PFK2 activation, whereas ectopic expression of circACC1 rescued these effects (Figure 6F). These findings therefore indicate that the expression and downstream actions of circACC1 are driven through JNK signaling.

### Biological Implications of CircACC1 in Tumorigenesis

Finally, we examined the significance of circACC1 in tumorigenesis. Consistent with the metabolic changes observed (Figures 2 and S2), silencing of circACC1 inhibited the proliferation of HCT116 cells (Figure 7A), whereas overexpression of circACC1, but not conditional binding mutants, enhanced cell proliferation (Figure 7B). The effects of circACC1 on cell viability were mirrored in the long-term survival of HCT116 cells in clonogenic assays with experiments performed with the conditional binding mutants of circACC1 (Figure S7A) along with knockdown of AMPK $\alpha$ , establishing that the effects of circACC1 on cell viability were through its regulation of AMPK (Figures S7B and S7C). We also examined whether growth inhibition after circACC1 knockdown was linked to increased ROS and decreased ATP production, the main end products of FAO and glycolysis. In clonogenic assays, treatment with either N-acetylcysteine (NAC) to inhibit ROS (Spagnuolo et al., 2006) or ATP to replenish depleted ATP levels (Chaudry, 1982; Qian et al., 2014) were each shown to partially rescue growth in cells with circACC1 knockdown (Figure 7C). Moreover, combining NAC and ATP treatments proved sufficient to restore colony formation in circACC1-depleted cells to near control levels. Similarly, evaluation of xenografted tumors in nu/nu mice demonstrated that depletion of circACC1 markedly retarded growth *in vivo*, while its enforced expression produced the opposite (Figures 7D and 7E, respectively). Thus, the levels of circACC1 can impart significant effects on tumor growth, mediated through AMPK-dependent changes in cell metabolism.

To examine if circACC1 levels are important in human cancers, we measured circACC1 expression in colorectal cancer tissues along with their paired adjacent non-cancerous tissues. There was differential expression between normal and cancerous tissues in the majority of cases, with 16 of 21 tumors expressing at least 2-fold higher levels of circACC1 (Figure 7F). Subsequent analysis indicated increased levels of phosphorylated c-Jun and AMPK along with higher levels of the AMPK subunits in the majority of cancers than normal tissues (Figures S7D and S7E). Correlation analyses also revealed a positive relationship between circACC1 expression and activated c-Jun along with the expression and activation of AMPK in tumors (Figure 7G).

## DISCUSSION

Reprogramming of energy metabolism is a hallmark of cancer and is thought to provide survival advantages for cancer cells under stress (Ward and Thompson, 2012). In a few examples, mutations in metabolic enzymes can transform cells, i.e., succinate dehydrogenase, fumarate hydratase, and isocitrate dehydrogenases (King et al., 2006; Reitman and Yan, 2010), but more

commonly, metabolic changes in cancers are driven by key oncogenes and tumor suppressors such as c-Myc, HIF-1 $\alpha$ , and p53 (Yeung et al., 2008). Nevertheless, there is considerable heterogeneity in the rewiring of cancer metabolism, and importantly, metabolic responses are strongly impacted by environmental cues. Within this field, there is a growing appreciation that ncRNAs, especially lncRNAs (Yang et al., 2014), also play critical roles in the regulation of altered cancer metabolism (Zhang et al., 2014). In the current study, we sought to characterize circRNAs involved in the regulation of lipid metabolism and energy homeostasis. We identified circACC1 as an activator of AMPK signaling, whose expression was elicited by metabolic stress conditions and function was to promote fatty acid  $\beta$ -oxidation and glycolysis.

CircACC1 was shown to bind to the regulatory  $\beta$ 1 and  $\gamma$ 1 subunits and, as a result of this interaction, promoted the assembly, stabilization, and activity of the AMPK holoenzyme. We also observed that unassociated subunits were subjected to ubiquitination and proteasomal degradation as previously observed (Crute et al., 1998; Hunter et al., 2014; Salatto et al., 2017). The same regulatory pressure on unassociated AMPK subunits is also likely to be responsible for the instability of AMPK complex observed when AMPK $\beta$  and  $\gamma$  were genetically deleted in mice (Cambridge et al., 2017; Foretz et al., 2011). We did not specifically investigate the specific ubiquitin ligases involved, but there are prior reports showing that AMPK subunits may be selectively targeted by different ubiquitin systems; for example, UBE2O acts as an E3 ligase for AMPK $\alpha$ 2 (Vila et al., 2017), the Laforin-Malin complex promotes ubiquitination of AMPK $\beta$  subunits (Moreno et al., 2010) as does the E3 ligase Cidea (Qi et al., 2008), while TRIM28 downregulates AMPK $\alpha$ 1 in human tumors (Pineda et al., 2015).

AMPK signaling is activated by upstream kinases that phosphorylate the catalytic subunit at Thr172, a key residue within an activation loop, causing a 100-fold enhancement of AMPK kinase activity (Hawley et al., 1996, 2005; Herrero-Martín et al., 2009; Shaw et al., 2004; Woods et al., 2003). Suppressing the expression of LKB1, CaMKK2, and TAK1 either alone or in combination showed that the circACC1-mediated augmentation of AMPK activity was co-dependent on these kinases. Our results propose that circACC1 promotes holoenzyme assembly and stability in concert with kinase-mediated activation of AMPK $\alpha$  on Thr172 phosphorylation to maintain AMPK activity under basal conditions. Nevertheless, underscoring the importance of circACC1, AMPK activity in the presence of AICAR was significantly less following depletion of circACC1, indicative of its contribution to the maximal activity of AMPK.

The binding of AMP to sites within AMPK $\gamma$  enhances AMPK activation 10-fold through an allosteric mechanism that prevents dephosphorylation of Thr172 (Xiao et al., 2011). The effects of circACC1 appeared analogous to the addition of the AMPK activator A-769662, which is known to function by stabilizing the interaction between the  $\alpha$ -subunit kinase domain and the carbohydrate-binding module at the N terminus of the  $\beta$ -subunit

(G) Correlation analyses conducted between circACC1 and the expression of the indicated proteins from (F).

Data in (A)–(F) are mean  $\pm$  SD; n = 3 independent experiments. (A and B) two-way ANOVA with Bonferroni's multiple comparison post-test; (C) one-way ANOVA with Tukey's multiple comparison post-test; (D–F) two-tailed paired Student's t test, ns, not significant, \*p < 0.05, \*\*p < 0.01, \*\*\*p < 0.001.

(G) R, Pearson correlation coefficients (r) and p values.

(Xiao et al., 2013). Alternatively, while circACC1 stabilizes complexes between AMPK $\beta$  and  $\gamma$  subunits, its functions are more pervasive, facilitating the stability and activity of the AMPK holoenzyme. Thus, it is tempting to speculate that activators such as A-769662 may mimic the actions of circACC1 to promote AMPK catalytic activity (Vincent et al., 2015).

We observed that circACC1 was induced after serum deprivation, a condition that decreases ATP synthesis and increases cellular ROS, factors known to cause metabolic stress and to be detrimental to cell survival (Huang et al., 2016; Lee et al., 2010). In this setting, circACC1 expression was elicited by c-Jun transactivation, part of the JNK-c-Jun signaling axis that is known to promote cell survival under metabolic stress. It is interesting that serum-deprivation stress, but not serine, glutamine, or glucose deprivation, was able to affect circACC1 expression. The reason for this is unclear but points to the existence of regulatory pathways corresponding to distinct metabolic stresses. Some or all of these stresses are experienced within growing tumors, and the perspective gained here indicates that circACC1 advantages the growth of tumors in mice.

Mechanistically, circACC1 is derived from the back-splicing of pre-ACC1 mRNA. Conventional RNA splicing generates a linear mRNA that can be translated into ACC1, but this process is subverted under serum-deprivation stress. As anticipated, the levels of pre-ACC1 RNA tracked with the increased circACC1 levels after serum deprivation, but the mechanisms governing the switch to circularization remain unknown. Nonetheless, it is reasonable to presume that under shortage of ATP, cells shut down anabolic processes that consume ATP. In this scenario, the ACC1 enzyme, which functions to provide the malonyl-CoA substrate for the biosynthesis of fatty acids, is not required. Rather, its production is sacrificed to increase the levels of circACC1, which in turn activates AMPK to promote  $\beta$ -oxidation. Why this mechanism has evolved is unclear, but there may be economic advantages for using splicing products as regulators, saving the energy used in the transcription and translation of ACC1. Moreover, it is intriguing that AMPK is also the key enzyme responsible for the inactivation of the ACC1 enzyme, and similarly, while the reasons are not yet known, such dual control mechanisms may allow cells to respond more timely to metabolic pressures.

In addition to the effects on promoting  $\beta$ -oxidation, we also observed changes in glycolysis. We found that overexpression of circACC1 promoted PFK2 activation and accelerated glycolysis, while conversely, circACC1 knockdown impeded glycolysis. There are presently conflicting reports as to how AMPK affects glycolysis, with findings suggesting that AMPK prevents glycolysis by inhibiting the expression of HIF-1 $\alpha$  (Faubert et al., 2013), whereas other studies determining that glycolysis is promoted by activation of PFKFB3 (Doménech et al., 2015; Marsin et al., 2000). We did not observe changes in HIF-1 $\alpha$  protein levels upon either circACC1 knockdown or overexpression, but rather, we found that circACC1-mediated activation of AMPK results in enhanced glycolysis through the activation of PFKFB3.

Finally, we demonstrate that the circACC1-mediated activation of AMPK observed in cell culture points to a likely pathological role in cancer. The role of AMPK in cancer continues to be controversial, with reports suggesting that AMPK can either suppress or enhance tumor growth (Eichner et al., 2019; Faubert et al., 2013), highlighting the contextual importance of individual

studies (Liang and Mills, 2013). We observed a positive relationship between circACC1 and cancer cell growth *in vitro* and *in vivo*, and notably, compared with their normal adjacent tissues, circACC1 expression was elevated in the majority of colorectal cancers. Moreover, positive correlations were observed between circACC1 levels, activation of c-Jun, and AMPK along with the levels of AMPK subunits in cancer tissues. This appears consistent with a prior study reporting that AMPK signaling was activated in approximately 60% of cases of colorectal cancer, albeit not as a standalone predictor of patient outcomes (Baba et al., 2010). However, while we did not determine if circACC1 levels were prognostic, a study of late-stage colorectal cancer patients reported that low AMPK activation in primary tumors correlated with worse outcomes following treatment with chemotherapy plus the vascular endothelial growth factor (VEGF) antagonist bevacizumab (Zulato et al., 2014). This appears to contradict our thesis that cancer cells gain survival advantages by upregulating AMPK activity. Nevertheless, it has been shown that bevacizumab itself induces activation of AMPK, leading to glucose depletion and ATP exhaustion in tumors (Nardo et al., 2011). This highlights the need to consider the contribution that anti-cancer treatments also play in reprogramming energy metabolism in cancer cells.

### Limitations of Study

Investigations are required to understand circACC1 function in the broader metabolic context, but the lack of a conserved circACC1 equivalent in mice imposes some restrictions. Moreover, from a mechanistic standpoint, while c-Jun is a major driver of circACC1 biogenesis, it is not clear how serum deprivation influences back-splicing events required to preferentially produce circACC1 over ACC1 mRNA. Finally, while our results propose that circACC1 functions to enhance AMPK activity via mimicking allosteric regulation, definitively understanding the mechanism of action will require crystallographic evidence.

### STAR★METHODS

Detailed methods are provided in the online version of this paper and include the following:

- KEY RESOURCES TABLE
- CONTACT FOR REAGENT AND RESOURCE SHARING
- EXPERIMENTAL MODEL AND SUBJECT DETAILS
  - Xenograft Model
  - Cell Lines and Tissues
  - CircRNA Expression Vectors
- METHOD DETAILS
  - RNA Interference
  - RNA Extraction and RNase R Treatment
  - Quantitative and Semi-quantitative RT-PCR
  - Nile Red Staining
  - *In Vitro* Transcription
  - Northern Blot
  - Western Blot and Immunoprecipitation
  - Total ATP, ROS, NADPH/NADP<sup>+</sup> Ratio and Lactate Measurements
  - Lipidomics and Free Fatty Acid Analyses
  - ECAR and FAO Rate Measurements

- Cytosolic/Nuclear Fractionation
- RNA FISH
- Biotin RNA Pull-down Assay
- Two-Step RNA-Binding Protein Immunoprecipitations
- Recombinant Protein Purification
- *In Vitro* Cyclization
- Ubiquitination Assay
- Electrophoretic Mobility Shift Assays
- Luciferase Reporter and Mammalian Two-Hybrid Assays
- AMPK Kinase Assay
- Absolute RNA Quantitation
- Chromatin Immunoprecipitation Assays
- Colony Formation Assay
- **QUANTIFICATION AND STATISTICAL ANALYSIS**
- **DATA AND SOFTWARE AVAILABILITY**

### SUPPLEMENTAL INFORMATION

Supplemental Information can be found online at <https://doi.org/10.1016/j.cmet.2019.05.009>.

### ACKNOWLEDGMENTS

We thank Prof. Zefeng Wang (CAS Key Lab for Computational Biology) for gifting the circRNA translation reporter. We are grateful to BioNovoGene (Suzhou) and Biotree (Shanghai) for assistance with LC-MS and GC-MS, respectively. This work was supported by the National Key R&D Program of China (2018YFA0107103, 2016YFC1302302), the National Natural Science Foundation of China (81820108021, 81430065, 31871437, and 21571095), and the NHMRC of Australia (1147271).

### AUTHOR CONTRIBUTIONS

Q.L., Y.W., R.F.T., X.D.Z., W.H., and M.W. designed the research. Q.L. performed most experiments and data analysis. Y.W., S.W., and Z.Z. conducted some experiments. X.D. collected tumor samples, and R.S. helped with Seahorse analysis. Q.L., M.W., R.F.T., and W.H. wrote the manuscript.

### DECLARATION OF INTERESTS

The authors declare no competing interests.

Received: October 22, 2018

Revised: March 11, 2019

Accepted: May 6, 2019

Published: May 30, 2019

### REFERENCES

- Altarejos, J.Y., and Montminy, M. (2011). CREB and the CREB co-activators: sensors for hormonal and metabolic signals. *Nat. Rev. Mol. Cell Biol.* **12**, 141–151.
- Ashwal-Fluss, R., Meyer, M., Pamudurti, N.R., Ivanov, A., Bartok, O., Hanan, M., Evtantal, N., Memczak, S., Rajewsky, N., and Kadener, S. (2014). circRNA biogenesis competes with pre-mRNA splicing. *Mol. Cell* **56**, 55–66.
- Baba, Y., Noshu, K., Shima, K., Meyerhardt, J.A., Chan, A.T., Engelman, J.A., Cantley, L.C., Loda, M., Giovannucci, E., Fuchs, C.S., et al. (2010). Prognostic significance of AMP-activated protein kinase expression and modifying effect of MAPK3/1 in colorectal cancer. *Br. J. Cancer* **103**, 1025–1033.
- Bensinger, S.J., and Christofk, H.R. (2012). New aspects of the Warburg effect in cancer cell biology. *Semin. Cell Dev. Biol.* **23**, 352–361.
- Cambridge, E.L., McIntyre, Z., Clare, S., Arends, M.J., Goulding, D., Isherwood, C., Caetano, S.S., Reviriego, C.B., Swiatkowska, A., Kane, L., et al. (2017). The AMP-activated protein kinase beta 1 subunit modulates erythrocyte integrity. *Exp. Hematol.* **45**, 64–68.e5.
- Carracedo, A., Cantley, L.C., and Pandolfi, P.P. (2013). Cancer metabolism: fatty acid oxidation in the limelight. *Nat. Rev. Cancer* **13**, 227–232.
- Chaudry, I.H. (1982). Does ATP cross the cell plasma membrane. *Yale J. Biol. Med* **55**, 1–10.
- Chen, X., Han, P., Zhou, T., Guo, X., Song, X., and Li, Y. (2016a). circRNADb: a comprehensive database for human circular RNAs with protein-coding annotations. *Sci. Rep.* **6**, 34985.
- Chen, Y.G., Kim, M.V., Chen, X., Batista, P.J., Aoyama, S., Wilusz, J.E., Iwasaki, A., and Chang, H.Y. (2017). Sensing self and foreign circular RNAs by intron identity. *Mol. Cell* **67**, 228–238.e5.
- Chen, Z., Li, J.L., Lin, S., Cao, C., Gimbrone, N.T., Yang, R., Fu, D.A., Carper, M.B., Haura, E.B., Schabath, M.B., et al. (2016b). cAMP/CREB-regulated LINC00473 marks LKB1-inactivated lung cancer and mediates tumor growth. *J. Clin. Invest.* **126**, 2267–2279.
- Chuang, T.J., Wu, C.S., Chen, C.Y., Hung, L.Y., Chiang, T.W., and Yang, M.Y. (2016). NCLScan: accurate identification of non-co-linear transcripts (fusion, trans-splicing and circular RNA) with a good balance between sensitivity and precision. *Nucleic Acids Res.* **44**, e29.
- Corton, J.M., Gillespie, J.G., Hawley, S.A., and Hardie, D.G. (1995). 5-Aminoimidazole-4-carboxamide ribonucleoside. A specific method for activating AMP-activated protein kinase in intact cells? *Eur. J. Biochem.* **229**, 558–565.
- Crute, B.E., Seefeld, K., Gamble, J., Kemp, B.E., and Witters, L.A. (1998). Functional domains of the  $\alpha$ 1 catalytic subunit of the AMP-activated protein kinase. *J. Biol. Chem.* **273**, 35347–35354.
- Currie, E., Schulze, A., Zechner, R., Walther, T.C., and Farese, R.V., Jr. (2013). Cellular fatty acid metabolism and cancer. *Cell Metab.* **18**, 153–161.
- Damiano, F., Alemanno, S., Gnoni, G.V., and Siculella, L. (2010). Translational control of the sterol-regulatory transcription factor SREBP-1 mRNA in response to serum starvation or ER stress is mediated by an internal ribosome entry site. *Biochem. J.* **429**, 603–612.
- Davies, S.P., Helps, N.R., Cohen, P.T., and Hardie, D.G. (1995). 5'-AMP inhibits dephosphorylation, as well as promoting phosphorylation, of the AMP-activated protein kinase. Studies using bacterially expressed human protein phosphatase-2C $\alpha$  and native bovine protein phosphatase-2AC. *FEBS Lett.* **377**, 421–425.
- Davis, R.J. (2000). Signal transduction by the JNK group of MAP kinases. *Cell* **103**, 239–252.
- Doménech, E., Maestre, C., Esteban-Martínez, L., Partida, D., Pascual, R., Fernández-Miranda, G., Seco, E., Campos-Olivas, R., Pérez, M., Megias, D., et al. (2015). AMPK and PFKFB3 mediate glycolysis and survival in response to mitophagy during mitotic arrest. *Nat. Cell Biol.* **17**, 1304–1316.
- Eichner, L.J., Brun, S.N., Herzig, S., Young, N.P., Curtis, S.D., Shackelford, D.B., Shokhirev, M.N., Leblanc, M., Vera, L.I., Hutchins, A., et al. (2019). Genetic analysis reveals AMPK is required to support tumor growth in murine Kras-dependent lung cancer models. *Cell Metab.* **29**, 285–302.e7.
- Enuka, Y., Lauriola, M., Feldman, M.E., Sas-Chen, A., Ulitsky, I., and Yarden, Y. (2016). Circular RNAs are long-lived and display only minimal early alterations in response to a growth factor. *Nucleic Acids Res.* **44**, 1370–1383.
- Faubert, B., Boily, G., Izreig, S., Griss, T., Samborska, B., Dong, Z., Dupuy, F., Chambers, C., Fuerth, B.J., Violette, B., et al. (2013). AMPK is a negative regulator of the Warburg effect and suppresses tumor growth in vivo. *Cell Metab.* **17**, 113–124.
- Folkman, J. (2003). Angiogenesis and apoptosis. *Semin. Cancer Biol.* **13**, 159–167.
- Foretz, M., Hébrard, S., Guihard, S., Leclerc, J., Do Cruzeiro, M.D., Hamard, G., Niedergang, F., Gaudry, M., and Violette, B. (2011). The AMPK $\gamma$ 1 subunit plays an essential role in erythrocyte membrane elasticity, and its genetic inactivation induces splenomegaly and anemia. *FASEB J.* **25**, 337–347.
- Fullerton, M.D., Galic, S., Marcinko, K., Sikkema, S., Pulnilkunnil, T., Chen, Z.P., O'Neill, H.M., Ford, R.J., Palanivel, R., O'Brien, M., et al. (2013). Single

- phosphorylation sites in Acc1 and Acc2 regulate lipid homeostasis and the insulin-sensitizing effects of metformin. *Nat. Med.* **19**, 1649–1654.
- Glazar, P., Papavasileiou, P., and Rajewsky, N. (2014). circBase: a database for circular RNAs. *RNA* **20**, 1666–1670.
- Godlewski, J., Nowicki, M.O., Bronisz, A., Nuovo, G., Palatini, J., De Lay, M., Van Brocklyn, J., Ostrowski, M.C., Chiocca, E.A., and Lawler, S.E. (2010). MicroRNA-451 regulates LKB1/AMPK signaling and allows adaptation to metabolic stress in glioma cells. *Mol. Cell* **37**, 620–632.
- Göransson, O., McBride, A., Hawley, S.A., Ross, F.A., Shpiro, N., Foretz, M., Viollet, B., Hardie, D.G., and Sakamoto, K. (2007). Mechanism of action of A-769662, a valuable tool for activation of AMP-activated protein kinase. *J. Biol. Chem.* **282**, 32549–32560.
- Hansen, T.B., Wiklund, E.D., Bramsen, J.B., Villadsen, S.B., Statham, A.L., Clark, S.J., and Kjems, J. (2011). miRNA-dependent gene silencing involving Ago2-mediated cleavage of a circular antisense RNA. *EMBO J.* **30**, 4414–4422.
- Hardie, D.G. (2011). AMP-activated protein kinase: an energy sensor that regulates all aspects of cell function. *Genes Dev.* **25**, 1895–1908.
- Hardie, D.G. (2013). AMPK: a target for drugs and natural products with effects on both diabetes and cancer. *Diabetes* **62**, 2164–2172.
- Hardie, D.G., and Ashford, M.L.J. (2014). AMPK: regulating energy balance at the cellular and whole body levels. *Physiology* **29**, 99–107.
- Hardie, D.G., and Pan, D.A. (2002). Regulation of fatty acid synthesis and oxidation by the AMP-activated protein kinase. *Biochem. Soc. Trans.* **30**, 1064–1070.
- Hardie, D.G., Ross, F.A., and Hawley, S.A. (2012a). AMP-activated protein kinase: a target for drugs both ancient and modern. *Chem. Biol.* **19**, 1222–1236.
- Hardie, D.G., Ross, F.A., and Hawley, S.A. (2012b). AMPK: a nutrient and energy sensor that maintains energy homeostasis. *Nat. Rev. Mol. Cell Biol.* **13**, 251–262.
- Hawley, S.A., Boudeau, J., Reid, J.L., Mustard, K.J., Udd, L., Mäkelä, T.P., Alessi, D.R., and Hardie, D.G. (2003). Complexes between the LKB1 tumor suppressor, STRAD $\alpha/\beta$  and MO25 $\alpha/\beta$  are upstream kinases in the AMP-activated protein kinase cascade. *J. Biol.* **2**, 28.
- Hawley, S.A., Davison, M., Woods, A., Davies, S.P., Beri, R.K., Carling, D., and Hardie, D.G. (1996). Characterization of the AMP-activated protein kinase kinase from rat liver and identification of threonine 172 as the major site at which it phosphorylates AMP-activated protein kinase. *J. Biol. Chem.* **271**, 27879–27887.
- Hawley, S.A., Pan, D.A., Mustard, K.J., Ross, L., Bain, J., Edelman, A.M., Frenguelli, B.G., and Hardie, D.G. (2005). Calmodulin-dependent protein kinase kinase- $\beta$  is an alternative upstream kinase for AMP-activated protein kinase. *Cell Metab.* **2**, 9–19.
- Herrero-Martín, G., Hoyer-Hansen, M., García-García, C., Fumarola, C., Farkas, T., López-Rivas, A., and Jäättelä, M. (2009). TAK1 activates AMPK-dependent cytoprotective autophagy in TRAIL-treated epithelial cells. *EMBO J.* **28**, 677–685.
- Huang, D., Li, T., Wang, L., Zhang, L., Yan, R., Li, K., Xing, S., Wu, G., Hu, L., Jia, W., et al. (2016). Hepatocellular carcinoma redirects to ketolysis for progression under nutrition deprivation stress. *Cell Res.* **26**, 1112–1130.
- Hunter, R.W., Foretz, M., Bultot, L., Fullerton, M.D., Deak, M., Ross, F.A., Hawley, S.A., Shpiro, N., Viollet, B., Barron, D., et al. (2014). Mechanism of action of compound-13: an  $\alpha$ 1-selective small molecule activator of AMPK. *Chem. Biol.* **21**, 866–879.
- Hurley, R.L., Anderson, K.A., Franzone, J.M., Kemp, B.E., Means, A.R., and Witters, L.A. (2005). The Ca<sup>2+</sup>/calmodulin-dependent protein kinase kinases are AMP-activated protein kinase kinases. *J. Biol. Chem.* **280**, 29060–29066.
- Jeon, S.M. (2016). Regulation and function of AMPK in physiology and diseases. *Exp. Mol. Med.* **48**, e245.
- Jeon, S.M., Chandel, N.S., and Hay, N. (2012). AMPK regulates NADPH homeostasis to promote tumour cell survival during energy stress. *Nature* **485**, 661–665.
- Jiang, B., Zhang, J., Xia, J., Zhao, W., Wu, Y., Shi, M., Luo, L., Zhou, H., Chen, A., Ma, H., et al. (2017). IDH1 mutation promotes tumorigenesis by inhibiting JNK activation and apoptosis induced by serum starvation. *Cell Rep.* **19**, 389–400.
- Jones, R.G., and Thompson, C.B. (2009). Tumor suppressors and cell metabolism: a recipe for cancer growth. *Genes Dev.* **23**, 537–548.
- Kahn, B.B., Alquier, T., Carling, D., and Hardie, D.G. (2005). AMP-activated protein kinase: ancient energy gauge provides clues to modern understanding of metabolism. *Cell Metab.* **1**, 15–25.
- King, A., Selak, M.A., and Gottlieb, E. (2006). Succinate dehydrogenase and fumarate hydratase: linking mitochondrial dysfunction and cancer. *Oncogene* **25**, 4675–4682.
- Lamph, W.W., Wamsley, P., Sassone-Corsi, P., and Verma, I.M. (1988). Induction of proto-oncogene JUN/AP-1 by serum and TPA. *Nature* **334**, 629–631.
- Lee, S.B., Kim, J.J., Kim, T.W., Kim, B.S., Lee, M.S., and Do Yoo, Y.D. (2010). Serum deprivation-induced reactive oxygen species production is mediated by Romo1. *Apoptosis* **15**, 204–218.
- Liang, J., and Mills, G.B. (2013). AMPK: a contextual oncogene or tumor suppressor? *Cancer Res.* **73**, 2929–2935.
- Lin, S.C., and Hardie, D.G. (2018). AMPK: sensing glucose as well as cellular energy status. *Cell Metab.* **27**, 299–313.
- Liu, X., Xiao, Z.D., Han, L., Zhang, J., Lee, S.W., Wang, W., Lee, H., Zhuang, L., Chen, J., Lin, H.K., et al. (2016). LncRNA NBR2 engages a metabolic checkpoint by regulating AMPK under energy stress. *Nat. Cell Biol.* **18**, 431–442.
- Lu, G.D., Ang, Y.H., Zhou, J., Tamilarasi, J., Yan, B., Lim, Y.C., Srivastava, S., Salto-Tellez, M., Hui, K.M., Shen, H.M., et al. (2015). CCAAT/enhancer binding protein  $\alpha$  predicts poorer prognosis and prevents energy starvation-induced cell death in hepatocellular carcinoma. *Hepatology* **61**, 965–978.
- Marsin, A.S., Bertrand, L., Rider, M.H., Deprez, J., Beauloye, C., Vincent, M.F., Van den Berghe, G., Carling, D., and Hue, L. (2000). Phosphorylation and activation of heart PFK-2 by AMPK has a role in the stimulation of glycolysis during ischaemia. *Curr. Biol.* **10**, 1247–1255.
- Marsin, A.S., Bouzin, C., Bertrand, L., and Hue, L. (2002). The stimulation of glycolysis by hypoxia in activated monocytes is mediated by AMP-activated protein kinase and inducible 6-phosphofructo-2-kinase. *J. Biol. Chem.* **277**, 30778–30783.
- Memczak, S., Jens, M., Elefsinioti, A., Torti, F., Krueger, J., Rybak, A., Maier, L., Mackowiak, S.D., Gregersen, L.H., Munschauer, M., et al. (2013). Circular RNAs are a large class of animal RNAs with regulatory potency. *Nature* **495**, 333–338.
- Moreno, D., Towler, M.C., Hardie, D.G., Knecht, E., and Sanz, P. (2010). The laforin–malin complex, involved in Lafora disease, promotes the incorporation of K63-linked ubiquitin chains into AMP-activated protein kinase  $\beta$  subunits. *Mol. Biol. Cell* **21**, 2578–2588.
- Nardo, G., Favaro, E., Curtarello, M., Moserle, L., Zulato, E., Persano, L., Rossi, E., Esposito, G., Crescenzi, M., Casanovas, O., et al. (2011). Glycolytic phenotype and AMP kinase modify the pathologic response of tumor xenografts to VEGF neutralization. *Cancer Res.* **71**, 4214–4225.
- Oakhill, J.S., Scott, J.W., and Kemp, B.E. (2012). AMPK functions as an adenylate charge-regulated protein kinase. *Trends Endocrinol. Metab.* **23**, 125–132.
- Pineda, C.T., Ramanathan, S., Tacer, K.F., Weon, J.L., Potts, M.B., Ou, Y.H., White, M.A., and Potts, P.R. (2015). Degradation of AMPK by a cancer-specific ubiquitin ligase. *Cell* **160**, 715–728.
- Qi, J., Gong, J., Zhao, T., Zhao, J., Lam, P., Ye, J., Li, J.Z., Wu, J., Zhou, H.M., and Li, P. (2008). Downregulation of AMP-activated protein kinase by Cidea-mediated ubiquitination and degradation in brown adipose tissue. *EMBO J.* **27**, 1537–1548.
- Qian, Y., Wang, X., Liu, Y., Li, Y., Colvin, R.A., Tong, L., Wu, S., and Chen, X. (2014). Extracellular ATP is internalized by macropinocytosis and induces intracellular ATP increase and drug resistance in cancer cells. *Cancer Lett.* **351**, 242–251.
- Reitman, Z.J., and Yan, H. (2010). Isocitrate dehydrogenase 1 and 2 mutations in cancer: alterations at a crossroads of cellular metabolism. *J. Natl. Cancer Inst.* **102**, 932–941.

- Rybak-Wolf, A., Stottmeister, C., Glazar, P., Jens, M., Pino, N., Giusti, S., Hanan, M., Behm, M., Bartok, O., Ashwal-Fluss, R., et al. (2015). Circular RNAs in the mammalian brain are highly abundant, conserved, and dynamically expressed. *Mol. Cell* **58**, 870–885.
- Salatto, C.T., Miller, R.A., Cameron, K.O., Cokorinos, E., Reyes, A., Ward, J., Calabrese, M.F., Kurumbail, R.G., Rajamohan, F., Kalgutkar, A.S., et al. (2017). Selective activation of AMPK  $\beta$ 1-containing isoforms improves kidney function in a rat model of diabetic nephropathy. *J. Pharmacol. Exp. Ther.* **361**, 303–311.
- Sanders, M.J., Ali, Z.S., Hegarty, B.D., Heath, R., Snowden, M.A., and Carling, D. (2007). Defining the mechanism of activation of AMP-activated protein kinase by the small molecule A-769662, a member of the thienopyridone family. *J. Biol. Chem.* **282**, 32539–32548.
- Shaw, R.J., Kosmatka, M., Bardeesy, N., Hurley, R.L., Witters, L.A., DePinho, R.A., and Cantley, L.C. (2004). The tumor suppressor LKB1 kinase directly activates AMP-activated kinase and regulates apoptosis in response to energy stress. *Proc. Natl. Acad. Sci. USA* **101**, 3329–3335.
- Spagnuolo, G., D'Antò, V., Cosentino, C., Schmalz, G., Schweikl, H., and Rengo, S. (2006). Effect of N-acetyl-L-cysteine on ROS production and cell death caused by HEMA in human primary gingival fibroblasts. *Biomaterials* **27**, 1803–1809.
- Sundqvist, A., Bengoechea-Alonso, M.T., Ye, X., Lukiyanchuk, V., Jin, J., Harper, J.W., and Ericsson, J. (2005). Control of lipid metabolism by phosphorylation-dependent degradation of the SREBP family of transcription factors by SCF(Fbw7). *Cell Metab.* **1**, 379–391.
- Suzuki, H., Zuo, Y., Wang, J., Zhang, M.Q., Malhotra, A., and Mayeda, A. (2006). Characterization of RNase R-digested cellular RNA source that consists of lariat and circular RNAs from pre-mRNA splicing. *Nucleic Acids Res.* **34**, e63.
- Vila, I.K., Yao, Y., Kim, G., Xia, W., Kim, H., Kim, S.J., Park, M.K., Hwang, J.P., González-Billalabeitia, E., Hung, M.C., et al. (2017). A UBE2O-AMPK $\alpha$ 2 axis that promotes tumor initiation and progression offers opportunities for therapy. *Cancer Cell* **31**, 208–224.
- Vincent, E.E., Coelho, P.P., Blagih, J., Griss, T., Viollet, B., and Jones, R.G. (2015). Differential effects of AMPK agonists on cell growth and metabolism. *Oncogene* **34**, 3627–3639.
- Wakil, S.J., and Abu-Elheiga, L.A. (2009). Fatty acid metabolism: target for metabolic syndrome. *J. Lipid Res.* **50**, S138–S143.
- Ward, P.S., and Thompson, C.B. (2012). Metabolic reprogramming: a cancer hallmark even warburg did not anticipate. *Cancer Cell* **21**, 297–308.
- Willows, R., Sanders, M.J., Xiao, B., Patel, B.R., Martin, S.R., Read, J., Wilson, J.R., Hubbard, J., Gamblin, S.J., and Carling, D. (2017). Phosphorylation of AMPK by upstream kinases is required for activity in mammalian cells. *Biochem. J.* **474**, 3059–3073.
- Woods, A., Cheung, P.C.F., Smith, F.C., Davison, M.D., Scott, J., Beri, R.K., and Carling, D. (1996). Characterization of AMP-activated protein kinase and subunits assembly of the heterotrimeric complex in vitro. *J. Biol. Chem.* **271**, 10282–10290.
- Woods, A., Dickerson, K., Heath, R., Hong, S.P., Momcilovic, M., Johnstone, S.R., Carlson, M., and Carling, D. (2005).  $Ca^{2+}$ /calmodulin-dependent protein kinase kinase- $\beta$  acts upstream of AMP-activated protein kinase in mammalian cells. *Cell Metab.* **2**, 21–33.
- Woods, A., Johnstone, S.R., Dickerson, K., Leiper, F.C., Fryer, L.G.D., Neumann, D., Schlattner, U., Wallimann, T., Carlson, M., and Carling, D. (2003). LKB1 is the upstream kinase in the AMP-activated protein kinase cascade. *Curr. Biol.* **13**, 2004–2008.
- Xiao, B., Sanders, M.J., Carmena, D., Bright, N.J., Haire, L.F., Underwood, E., Patel, B.R., Heath, R.B., Walker, P.A., Hallen, S., et al. (2013). Structural basis of AMPK regulation by small molecule activators. *Nat. Commun.* **4**, 3017.
- Xiao, B., Sanders, M.J., Underwood, E., Heath, R., Mayer, F.V., Carmena, D., Jing, C., Walker, P.A., Eccleston, J.F., Haire, L.F., et al. (2011). Structure of mammalian AMPK and its regulation by ADP. *Nature* **472**, 230–233.
- Xie, M., Zhang, D., Dyck, J.R.B., Li, Y., Zhang, H., Morishima, M., Mann, D.L., Taffet, G.E., Baldini, A., Khoury, D.S., et al. (2006). A pivotal role for endogenous TGF- $\beta$ -activated kinase-1 in the LKB1/AMP-activated protein kinase energy-sensor pathway. *Proc. Natl. Acad. Sci. USA* **103**, 17378–17383.
- Yang, F., Zhang, H., Mei, Y., and Wu, M. (2014). Reciprocal regulation of HIF-1 $\alpha$  and lincRNA-p21 modulates the Warburg effect. *Mol. Cell* **53**, 88–100.
- Yang, Y., Fan, X., Mao, M., Song, X., Wu, P., Zhang, Y., Jin, Y., Yang, Y., Chen, L.L., Wang, Y., et al. (2017). Extensive translation of circular RNAs driven by N<sup>6</sup>-methyladenosine. *Cell Res.* **27**, 626–641.
- Yeung, S.J., Pan, J., and Lee, M.H. (2008). Roles of p53, MYC and HIF-1 in regulating glycolysis—the seventh hallmark of cancer. *Cell. Mol. Life Sci.* **65**, 3981–3999.
- Yu, C.Y., Li, T.C., Wu, Y.Y., Yeh, C.H., Chiang, W., Chuang, C.Y., and Kuo, H.C. (2017). The circular RNA circBIRC6 participates in the molecular circuitry controlling human pluripotency. *Nat. Commun.* **8**, 1149.
- Zhang, A., Xu, M., and Mo, Y.Y. (2014). Role of the lincRNA-p53 regulatory network in cancer. *J. Mol. Cell. Biol.* **6**, 181–191.
- Zhang, Y., Zhang, X.O., Chen, T., Xiang, J.F., Yin, Q.F., Xing, Y.H., Zhu, S.S., Yang, L., and Chen, L.L. (2013). Circular intronic long noncoding RNAs. *Mol. Cell* **51**, 792–806.
- Zulato, E., Bergamo, F., De Paoli, A., Griguolo, G., Esposito, G., De Salvo, G.L., Mescoli, C., Rugge, M., Nardin, M., Di Grazia, L., et al. (2014). Prognostic significance of AMPK activation in advanced stage colorectal cancer treated with chemotherapy plus bevacizumab. *Br. J. Cancer* **111**, 25–32.
- Zungu, M., Schisler, J.C., Essop, M.F., McCudden, C., Patterson, C., and Willis, M.S. (2011). Regulation of AMPK by the ubiquitin proteasome system. *Am. J. Pathol.* **178**, 4–11.

## STAR★METHODS

## KEY RESOURCES TABLE

REAGENT or RESOURCE	SOURCE	IDENTIFIER
<b>Antibodies</b>		
p-ACC ser79 (WB 1:1000)	CST	Cat#3661; RRID:AB_330337
ACC1 (WB 1:1000)	CST	Cat#4190; RRID:AB_10547752
β-actin (WB 1:1000)	CST	Cat#3700; RRID:AB_2242334
PARP (WB 1:1000)	CST	Cat#9532; RRID:AB_659884
p-AMPK Thr172 (WB 1:1000)	CST	Cat#2535; RRID:AB_331250
AMPKα1 (WB 1:500)	CST	Cat#2795; RRID:AB_560856
AMPKα2 (WB 1:1000)	CST	Cat#2757; RRID:AB_560858
AMPKβ1 (WB 1:2000; IP 1:100)	Proteintech Group	Cat#10308-1-AP; RRID:AB_513239
AMPKγ1 (IP 1:50)	Abcam	Cat#ab32508; RRID:AB_722769
AMPKγ1 (WB 1:2000)	Proteintech Group	Cat#10290-1-AP; RRID:AB_2268781
p-PFKFB3 ser461 (WB 1:500)	Abcam	Cat#ab202291
PFKFB3 (WB 1:1000)	Proteintech Group	Cat#13763-1-AP; RRID:AB_2162854
HSP90 (WB 1:1000)	CST	Cat#4877; RRID:AB_2233307
HUR (WB 1:1000)	CST	Cat#12582
Flag-Tag (WB 1:2500)	Sigma	Cat#F3040; RRID:AB_439712
HA-Tag (WB 1:5000; IP 1:100)	Sigma	Cat#H9658; RRID:AB_260092
Ubiquitin (WB 1:1000)	CST	Cat#3936; RRID:AB_331292
LKB1 (WB 1:1000)	Proteintech Group	Cat#10746-1-AP; RRID:AB_2271311
CaMKK2 (WB 1:1000)	Proteintech Group	Cat#11549-1-AP; RRID:AB_2259441
c-Jun (WB 1:1000)	Proteintech Group	Cat#24909-1-AP
TAK1 (WB 1:1000)	CST	Cat#5206; RRID:AB_10694079
p-c-Jun Ser73 (WB 1:1000; ChIP 1:50)	CST	Cat#3270; RRID:AB_2129575
p-JNK Thr183/185 (WB 1:1000)	CST	Cat#4668; RRID:AB_823588
JNK (WB 1:1000)	CST	Cat#9252; RRID:AB_2250373
SREBF1 (WB 1:1000)	Proteintech Group	Cat#14088-1-AP; RRID:AB_2255217
CREB1 (WB 1:1000)	Proteintech Group	Cat#12208-1-AP; RRID:AB_2245417
CEBPA (WB 1:1000)	Proteintech Group	Cat#18311-1-AP; RRID:AB_2077892
GFP (WB 1:2000)	Abmart	Cat#M20004; RRID:AB_2619674
<b>Chemicals, Peptides, and Recombinant Proteins</b>		
ActD (actinomycin D)	MedChemExpress	Cat#HY-17559; CAS:50-76-0
A-769662	MedChemExpress	Cat#HY-50662; CAS: 844499-71-4
AICAR	MedChemExpress	Cat# HY-13417; CAS: 50-76-0
DB07268	MedChemExpress	Cat#HY-15737; CAS: 929007-72-7
Carnitine	MedChemExpress	Cat#HY-B0399 ; CAS: 541-15-1
MG132	Sigma	Cat#M8699; CAS: 1211877-36-9
Cycloheximide	Calbiochem	Cat#239763; CAS: 66-81-9
3xFlag Peptides	APExBIO	Cat#A6001
HA Peptides	APExBIO	Cat#A6004
<b>Critical Commercial Assays</b>		
DMEM	Gibco	Cat#12800082
RPMI-1640	Gibco	Cat#61870044
DMEM, no Glucose	Gibco	Cat#11966025
DMEM, no glucose, no glutamine	Gibco	Cat#A1443001
TRIZOL	Invitrogen	Cat#AM9738

(Continued on next page)

**Continued**

REAGENT or RESOURCE	SOURCE	IDENTIFIER
RNase R	Epicentre	Cat#RNR07250
PrimeScript™ RT reagent Kit	Takara	Cat#RR037A
SYBR Green 2xTaq mix	Takara	Cat#RR820A
2xTaq PCR mix	Vazyme	Cat#P212-01
Nile red	Sigma-Aldrich	Cat#72485
T7-Flash BiotinRNA Transcription Kit	Epicentre	Cat#ASB71110
TranscriptAid T7 High Yield Transcription Kit	Thermo Scientific	Cat#K0441
DIG Northern Starter Kit	Roche	Cat#12039672910
ATP assay kit	Beyotime	Cat#S0026
ROS Assay kit	Beyotime	Cat#S0033
NADP/NADPH Assay kit	Abcam	Cat#ab65349
Lactate Assay Kit	Sigma-Aldrich	Cat#MAK064
Seahorse XF Glycolysis Stress Test Kit	Agilent	Cat#103020-100
Seahorse XF Cell Mito Stress Test Kit	Agilent	Cat#103015-100
XF Palmitate-BSA FAO Substrate	Agilent	Cat#102720-100
ULYSIS® Nucleic Acid Labeling Kit	Thermo Fisher	Cat#U21652
Dynabeads™ M-280 Streptavidin	Invitrogen	Cat#60210
Pierce™ Protein A/G UltraLink™ Resin	Thermo Scientific	Cat#53133
GST-tagged protein purification kit	Beyotime	Cat#P2262
T4 DNA ligase	NEB	Cat#M0202M
RIPA buffer	Beyotime	Cat#P0013B
LightShift™ Chemiluminescent RNA EMSA Kit	Thermo Scientific	Cat#20158
Dual-Luciferase® Reporter Assay System	Promega	Cat#E1910
EZ ChIP™ Chromatin Immunoprecipitation Kit	Millipore	Cat#17-371RF
<b>Deposited Data</b>		
Raw Data	This paper	<a href="https://doi.org/10.17632/79kfhcvbmt.1">https://doi.org/10.17632/79kfhcvbmt.1</a>
<b>Experimental Models: Cell Lines</b>		
HCT116	ATCC	CCL-247
293T	ATCC	CRL-3216
HeLa	ATCC	CCL-2
A549	ATCC	CCL-185
HepG2	ATCC	HB-8065
HT29	ATCC	HTB-38
U2OS	ATCC	HTB-96
H1299	Shanghai Cell Bank (CAS, Shanghai, China)	TCHu160
MCF7	Shanghai Cell Bank (CAS, Shanghai, China)	SCSP-531
Hep3B	Laboratory of Ping Gao (USTC)	N/A
HAFF	This paper	N/A
LO2	Shanghai Cell Bank (CAS, Shanghai, China)	GNHu 6
<b>Oligonucleotides</b>		
shRNA sequences	see <a href="#">Table S1</a>	N/A
Biotin labelled probes sequences	see <a href="#">Table S1</a>	N/A
Primers used in qRT-PCR & Semi-quantitative RT-PCR analysis	see <a href="#">Table S1</a>	N/A
Primers for in vitro transcription	see <a href="#">Table S1</a>	N/A
DNA splints for in vitro cyclization	see <a href="#">Table S1</a>	N/A

(Continued on next page)

**Continued**

REAGENT or RESOURCE	SOURCE	IDENTIFIER
FISH & Northern blot probe sequence for circACC1	see <a href="#">Table S1</a>	N/A
Insertion Sequence of IRES-reporter plasmid	see <a href="#">Table S1</a>	N/A
<b>Recombinant DNA</b>		
pCDH-circRNA-empty	This paper	N/A
pCDH-circACC1	This paper	N/A
pCDH-circACC1R	This paper	N/A
pCDH-circACC1ΔP1a	This paper	N/A
pCDH-circACC1ΔP1b	This paper	N/A
p3xFLAG-AMPK $\alpha$ 1	This paper	N/A
p3xFLAG-AMPK $\beta$ 1	This paper	N/A
p3xFLAG-AMPK $\gamma$ 1	This paper	N/A
pGEX-GST-AMPK $\alpha$ 1	This paper	N/A
pGEX-GST-AMPK $\beta$ 1	This paper	N/A
pGEX-GST-AMPK $\gamma$ 1	This paper	N/A
pGEX-GST-ACC1-1-130aa	This paper	N/A
p3xFLAG-AMPK $\beta$ 1-CBM	This paper	N/A
p3xFLAG-AMPK $\beta$ 1-CTD	This paper	N/A
p3xFLAG-AMPK $\beta$ 1- $\Delta\alpha\gamma$ BD2	This paper	N/A
p3xFLAG-AMPK $\gamma$ 1-BD1	This paper	N/A
p3xFLAG-AMPK $\gamma$ 1-BD2	This paper	N/A
p3xFLAG-AMPK $\gamma$ 1- $\Delta$ BD2	This paper	N/A
pCMV-HA-AMPK $\beta$ 1	This paper	N/A
pCMV-HA-AMPK $\gamma$ 1	This paper	N/A
pBIND-AMPK $\beta$ 1	This paper	N/A
pBIND-AMPK $\gamma$ 1	This paper	N/A
pACT-AMPK $\alpha$ 1	This paper	N/A
pACT-AMPK $\beta$ 1	This paper	N/A
pCDH-3xFlag-AMPK $\alpha$ 1-CA(1-312aa,T172D)	This paper	N/A
pGL3-ACC1-promoter	This paper	N/A
pGL3-ACC1-mut-promoter	This paper	N/A
p3xFLAG-c-Jun	This paper	N/A
pLKO.1-puro	Sigma	SHC002
pCirc-IRES-reporter	Prof. Zefeng Wang (CAS Key Lab for Computational Biology)	N/A
<b>Software and Algorithms</b>		
GraphPad Prism 6	GraphPad Software	<a href="https://www.graphpad.com/">https://www.graphpad.com/</a>
ImageJ	NIH, USA	<a href="https://imagej.nih.gov/ij/">https://imagej.nih.gov/ij/</a>

**CONTACT FOR REAGENT AND RESOURCE SHARING**

Further information and requests for resources and reagents should be directed to and will be fulfilled by the Lead Contact, Mian Wu ([wumian@ustc.edu.cn](mailto:wumian@ustc.edu.cn)).

**EXPERIMENTAL MODEL AND SUBJECT DETAILS****Xenograft Model**

The Balb/c nude mice (4 weeks old, ♂) were obtained from Beijing Vital River Laboratory Animal Technology Co., Ltd and housed in a specific pathogen free facility. Cells were injected subcutaneously into the dorsal flanks of nu/nu mice ( $3 \times 10^6$  cells for sh-ctrl and

sh-circACC1 or  $2 \times 10^6$  for pCDH and pCDH-circACC1 HCT116 cells) and after 21 days, mice were sacrificed and tumors were excised and weighed. Studies were conducted with approval from the Animal Research Ethics Committee of University of Science and Technology of China.

### Cell Lines and Tissues

The LO2 cell line (unknown sex) was cultured in RPMI-1640 (Gibco), 10% FBS and maintained at 37°C in 5% CO<sub>2</sub> whereas all other lines (HCT116 (♂), 293T (♀), HeLa (♀), A549 (♂), HepG2 (♂), HT29 (♀), U2OS (♀), H1299 (♂), MCF7 (♀), Hep3B (♂), HAFF (♂)) were cultured DMEM containing 10% FBS and 1% sodium pyruvate. Freshly removed cancer and adjacent non-cancerous colon tissues were obtained from surgical resections undertaken at the Department of General Surgery at First Affiliated Hospital of Anhui Medical University. All samples were collected with the informed consent of patients. The studies complied with all relevant ethical regulations and were conducted under approvals from the Human Research Ethics Committees of the University of Science and Technology of China and the First Affiliated Hospital of Anhui Medical University in agreement with the guidelines set forth by the Declaration of Helsinki. Subject details are shown in [Table S2](#).

### CircRNA Expression Vectors

Two tandem reverse complementary intron sequences were first inserted into pCDH-CMV-MCS-EF1-Puro (SBI). The mature circACC1 sequence was PCR amplified and inserted into the region between the two introns to provide AG receptor and GT donor pairing. Cyclization was confirmed by divergent primers and SJOD primer (Splice Junction Overlapping Divergent Primers) and the accuracy of conjunction confirmed by Sanger sequencing. To examine translation potential, the predicted potential IRES of circACC1 (64–175 bp) was inserted into the pCirc-GFP-IRES circRNA translation reporter containing a split GFP system using EcoRI and EcoRV (a kind gift of Prof. Zefeng Wang, CAS Key Lab for Computational Biology). Primer sequences used or construct sequences are shown in [Table S1](#).

## METHOD DETAILS

### RNA Interference

Lentiviruses for gene knockdown experiments were generated by transfecting HEK293T cells for 48 h with PLKO.1 based shRNAs, pREV, pGag and pVSVG at the ratio of 2:2:2:1. Lentiviral supernatant were filtered by 0.45 μm filter before target cells infection. Stably transduced cell lines were selected with 1 μg/ml puromycin. Targeting sequences are shown in [Table S1](#).

### RNA Extraction and RNase R Treatment

Total RNA was isolated using TRIzol followed by DNase-treatment. RNA samples were incubated 15 min at 37°C with 3 U/μg or without RNase R before subsequent recovery using phenol-chloroform extraction.

### Quantitative and Semi-quantitative RT-PCR

One μg RNA was used to synthesize cDNA using PrimeScript™ RT reagent kit (TaKaRa) according to the manufacturer's instructions. Semi-quantitative RT-PCR was performed using 2x Taq PCR mix with 25 cycles for internal controls and 30–40 cycles for circRNAs. Primer sequences are shown in [Table S1](#).

### Nile Red Staining

Cells were washed using PBS, fixed using 4% formaldehyde solution and stained for 10 min with 0.05 μg/ml Nile red solution to visualize lipid droplets. Cell nuclei were counterstained DAPI and images acquired by laser confocal microscopy (Zeiss LSM880).

### In Vitro Transcription

The DNA template used for *in vitro* synthesis of biotinylated circACC1 was generated by PCR. The forward primer contained the T7 RNA polymerase promoter sequence to allow for subsequent *in vitro* transcription. PCR products were purified using the DNA Gel Extraction Kit (Axygen), and *in vitro* transcription was performed using the T7-Flash BiotinRNA Transcription Kit (Epicentre, biotin labelling) or TranscriptAid T7 High Yield Transcription Kit (Thermo Scientific, without biotin) according to the manufacturer's instructions. RNA was subsequently purified by phenol-chloroform extraction. Primer sequences are shown in [Table S1](#).

### Northern Blot

Ten μg of total RNA was resolved on 1% denaturing agarose gels before transfer to Hybond-N (GE). Membranes were then dried and UV-crosslinked (200,000 μJ/cm<sup>2</sup> at 265 nm). Digoxin-labelled RNA probes ([Table S1](#)) were prepared using the DIG Northern Starter Kit (Roche) and incubated with membranes overnight at 55°C before visualizing bands using an Image Quant LAS-4000 mini (GE Fujifilm).

### Western Blot and Immunoprecipitation

Whole cell lysates were prepared using RIPA buffer containing protease inhibitors (Beyotime). After boiling, the supernatants were subjected to SDS-PAGE and transferred to nitrocellulose membranes. After blocking with 5% non-fat milk, membranes

were successively incubated with primary and HRP-conjugated secondary antibodies before visualizing bands using enhanced chemiluminescence (Tanon 5200). For immunoprecipitation, cells were lysed in IP lysis buffer (0.5% NP-40, 150 mM NaCl, 20 mM HEPES, pH 7.4, 2 mM EDTA, and 1.5 mM MgCl<sub>2</sub>) supplemented with protease inhibitor cocktail for 40 min on ice. Cell lysates were incubated with the indicated antibodies adsorbed to protein A/G-sepharose beads for 4 h at 4°C before washing three times in IP lysis buffer and elution at 95°C for 10 min. Antibodies and dilutions used are shown in the [Key Resources Table](#).

### Total ATP, ROS, NADPH/NADP<sup>+</sup> Ratio and Lactate Measurements

Cellular ATP, ROS and intracellular NADPH, extracellular lactate levels was measured using the ATP assay (Beyotime), ROS Assay (Beyotime), NADPH/NADP<sup>+</sup> ratio assay (Abcam) kits and Lactate production assay (Sigma), respectively, according to the manufacturer's instructions.

### Lipidomics and Free Fatty Acid Analyses

For LC-MS, 10<sup>7</sup> cells were collected and flash-frozen in liquid nitrogen before extracting metabolites in chloroform/methanol (2/1, v/v). Samples were resolved using an Accucore C18 HPLC column (2.1 x 150 mm, 2.6 μm) on a Thermo Scientific Q Exactive Plus system with peaks analyzed and identified using LipidSearch software. For GC-MS-based free fatty acid measurements, cells were extracted in a 3:3:2 v/v mixture of acetonitrile, isopropanol and water before drying in a vacuum concentrator without heat. Samples were dissolved in methyl ester solution (methanol: sulfuric acid, 15:1 v/v) for 1 h at 90°C before twice extracting with hexane, blow drying with nitrogen and dissolution in isooctane. All samples (including standard FFAs) were analyzed using a SP2560 capillary column on a SHIMADAZU 2010 PLUS GC/MS system. Peaks representing each metabolite were extracted and analyzed according to standard FFAs peaks.

### ECAR and FAO Rate Measurements

Assays were performed using the Seahorse XFe96 analyzer (Seahorse Bioscience, Agilent) according to the manufacturer's instructions. Briefly, 1–2 x 10<sup>4</sup> cells/well were seeded in a 96-well XF cell culture microplate in growth medium 24 h before assay. ECAR was measured with an XF96 analyzer in XF base medium (pH 7.4) containing 1 mM glutamine following sequential additions of glucose (10 mM), oligomycin (1 μM) and 2-DG (50 mM). Data were analyzed by the Seahorse XF Glycolysis Stress Test Report Generator package. Alternatively, analyses of FAO rates were performed using the Seahorse XF Cell Mito Stress Test. Twenty four hours after seeding the cell culture medium was replaced with substrate-limited DMEM supplemented with 0.5 mM glucose, 1 mM glutamax, 0.5 mM carnitine, 1% FBS. After a further 24 h the medium was exchanged with FAO assay medium (KHB buffer:111 mM NaCl, 4.7 mM KCl, 1.25 mM CaCl<sub>2</sub>, 2 mM MgSO<sub>4</sub>, 1.2 mM NaH<sub>2</sub>PO<sub>4</sub> supplemented with 2.5 mM glucose, 0.5 mM carnitine and 5 mM HEPES, adjusted to pH 7.4 in 37°C). To examine free fatty acid oxidation, BSA-conjugated palmitate (XF Palmitate-BSA FAO Substrate) was added to a final concentration of 50 μM. Data were analyzed by the Seahorse XF Cell Mito Stress Test Report Generator package.

### Cytosolic/Nuclear Fractionation

Cells were resuspended in hypotonic buffer (25 mM Tris-HCl, PH 7.4, 1 mM MgCl<sub>2</sub>, 5 mM KCl) and incubated on ice for 5 min before adding an equal volume of hypotonic buffer containing 1% NP-40 for a further 5 min. After centrifuging the cells at 5,000 g for 5 min, the supernatant was collected as the Cytosolic fraction. The pellets were washed twice with hypotonic buffer, and then re-suspended in nuclear resuspension buffer (20 mM HEPES, pH 7.9, 400 mM NaCl, 1 mM EDTA, 1 mM EGTA, 1 mM DTT, 1 mM PMSF). After incubation on ice for 30 min, the sample was centrifuged at 12,000 g for 10 min and the supernatant collected as the Nuclear fraction. PARP, Hsp90 and U1 served as controls.

### RNA FISH

Complementary probes targeting the “head-to-tail” sequence were used to visualise circACC1 *in situ* (Table S1). RNA probes synthesized by T7-mediated transcription were subsequently purified by phenol-chloroform extraction and 1 μg RNA labelled with Alexa Fluor<sup>®</sup> 546 dye using the ULYSIS<sup>®</sup> Nucleic Acid Labeling Kit (Thermo Fisher). Cells were first fixed with methanol and acetic acid (3:1) for 10 min. After prehybridization (1 xPBS/0.5% Triton X-100), cells were hybridized with labelled RNA probes in hybridization buffer (50% formamide, 1x Denhardt's solution, 10% Dextran sulfate, 2x SSC, 10 mM EDTA (pH 8.0), 1 mg/ml yeast transfer RNA, 1 mg/ml sheared salmon sperm DNA) at 55°C overnight. Nuclei were counterstained with DAPI and images acquired by laser confocal microscopy (Zeiss LSM880).

### Biotin RNA Pull-down Assay

Cell lysates were prepared by ultrasonication in RIP buffer (150 mM KCl, 25 mM Tris (pH 7.4), 0.5 mM dithiothreitol, 0.5% NP-40, complete protease inhibitors cocktail and RNase inhibitors) and pre-cleared against streptavidin magnetic beads (Invitrogen). *In vitro* transcribed biotin-labelled RNA or DNA probes adsorbed to streptavidin magnetic beads were then incubated with cell lysates at 4 °C for 4 h before washing five times in RIP buffer and elution in Laemmli sample buffer. HuR was used as control RNA binding protein in the indicated assays.

### Two-Step RNA-Binding Protein Immunoprecipitations

All steps were performed under RNase free conditions. Cell lysates prepared using lysis buffer containing 20 mM HEPES (pH 7.8), 400 mM KCl, 5% glycerol, 5 mM EDTA, 1% NP40, protease inhibitors cocktail and RNase inhibitor were first immunoprecipitated with anti-Flag antibodies before elution with Flag peptides. Ten percent of the sample was reserved for Western blotting and semi-quantitative RT-PCR analysis, respectively, while the remaining eluate was further incubated with control IgG or anti-HA antibodies for the second phase immunoprecipitation.

### Recombinant Protein Purification

HA-tagged or Flag-tagged AMPK subunits expressed in 293T cells were purified using A/G-Sepharose bead-bound antibodies against HA or Flag. The immunoprecipitates were then eluted with indicated HA or 3x Flag peptides. GST-ACC1 (1-130 aa) was purified from *E.coli* using glutathione Sepharose (Beyotime) and dialyzed against 20 mM Tris-HCl, pH 8.0 and 10% glycerol at 4°C overnight.

### In Vitro Cyclization

*In vitro* cyclization of linear RNA was performed according to Howard Y. Chang with minor modifications (Chen et al., 2017). To assemble pre-ligation complexes, biotin-labelled or unlabeled RNA was incubated with the indicated DNA splints (molar ratio=1:1.5) at 90°C with shaking for 2 min before cooling the sample to room temperature over 15 min. Ligation to form circRNAs was then performed overnight at 16°C with T4 DNA ligase (NEB), followed by RNase R and DNase I treatment at 37°C for 30 min. RNA was subsequently purified by phenol-chloroform extraction. Primer and DNA splint sequences are shown in Table S1.

### Ubiquitination Assay

Cells were extracted in 200  $\mu$ l RIPA buffer (Beyotime) were heated for 10 min at 95°C, followed by sonication and dilution with 800  $\mu$ l of 10 mM Tris-HCl, pH 8.0, 150 mM NaCl, 2 mM EDTA, 1% Triton X-100. After incubation at 4°C for 30 min, samples were centrifuged at 20,000 g for 20 min and the clarified supernatants incubated with protein A/G-sepharose beads pre-adsorbed with the indicated antibodies for 4 h at 4°C. After washing three times using 10 mM Tris-HCl, pH 8.0, 1 M NaCl, 1 mM EDTA, 1% NP-40, proteins were eluted at 95°C for 10 min and analyzed by SDS-PAGE followed by Western blot.

### Electrophoretic Mobility Shift Assays

EMSA were performed using the LightShift Chemiluminescent RNA EMSA Kit according to the manufacturer's protocol (Thermo Scientific). Briefly, biotin labelled *in vitro* cyclized circACC1 RNA (BL circACC1, 2 nM) was incubated together with Flag-AMPK $\alpha$ 1,  $\beta$ 1 or  $\gamma$ 1 proteins. Unlabeled cyclized circACC1 (10  $\mu$ M) was used as competitor. Reactions were subjected to PAGE using native gels and after transfer to nylon membranes, the biotin labelled RNA was detected using SA-HRP and ECL.

### Luciferase Reporter and Mammalian Two-Hybrid Assays

Assays were performed according to the manufacturer's instructions (Promega) after transfection of the indicated plasmids. For the mammalian two-hybrid assay, complementary DNAs for AMPK $\alpha$ 1, AMPK $\beta$ 1 and AMPK $\gamma$ 1 were cloned into the pBIND and pACT vectors and transfected along with firefly (pG5luc) (Promega) luciferase vectors. Reporter activities were measured 24 and 48 h later, respectively for the luciferase reporter and mammalian two-hybrid assays using the Dual-Luciferase Reporter Assay Kit (Promega). Renilla measurements were used to normalize changes in firefly luciferase activity.

### AMPK Kinase Assay

Purified AMPK subunits were combined as indicated with 1  $\mu$ g GST-ACC1, 10  $\mu$ g of cyclized circACC1 or antisense circACC1, in the presence of 500  $\mu$ M ATP. The reaction mixture was kept at 30°C for 30 min followed by heating at 95°C for 10 min. Boiled samples were then analyzed on SDS-PAGE followed by Western blot.

### Absolute RNA Quantitation

Absolute RNA quantitation was performed by digital droplet PCR assay according to the manufacturer's instructions (Bio-Rad). RNA prepared from a defined number of cells was pre-digested with RNase R before synthesising cDNA as described for the RT-PCR assays. PCR reactions were reconstituted to a final volume of 20  $\mu$ l using ddPCR Supermix (Bio-Rad) and subsequently diluted before droplet formation and cycling to end point. Samples were then read using a Bio-Rad QX100 reader. Data generated as copies per  $\mu$ l were converted to copies per cell based on the cell input equivalents.

### Chromatin Immunoprecipitation Assays

Chromatin immunoprecipitation assays were performed by using the Millipore ChIP kit according to the manufacturer's instructions. Bound DNA fragments were subjected to real-time or semi-quantitative RT-PCR using specific primers (Table S1). Primers amplifying target sequences in the MMP1 and GAPDH promoters were used as a positive and negative controls, respectively.

**Colony Formation Assay**

Cells were seeded into 6-well plates (800–1000 cells/well) and two weeks later, fixed and stained with crystal violet. The percentage and intensity of the area covered by stained cell colonies were estimated using the ImageJ-plugin “ColonyArea”.

**QUANTIFICATION AND STATISTICAL ANALYSIS**

All cell and biochemical assays were repeated a minimum of three times with unequivocal results obtained. The experiments involving human tissues and xenografts were repeated twice. Statistical analysis was carried out using Microsoft Excel software and GraphPad Prism to assess the differences between experimental groups. Data were analysed by two-tailed Student’s t-test for comparisons of two samples, one-way ANOVA with Tukey’s post-test for univariate comparisons, two-way ANOVA with Bonferroni’s post-test for bivariate comparisons, or the Pearson coefficient for the linear correlation between two variables. Based on our prior experience with these techniques, no particular methods were used to determine whether data met the assumptions of the statistical tests. The statistical parameters can be found in the figure legends where values less than 0.05 were considered to be statistically significant.

**DATA AND SOFTWARE AVAILABILITY**

Unprocessed original image data have been deposited to Mendely Data and are available at: <https://doi.org/10.17632/79kfhcvtbmt.1>.